

N81-20462 UNCLAS



19951226 010

DEPARTMENT OF DEFENSE
PLASTIC TECHNICAL EVALUATION CENTER
STRADCOM, COVER, N. I. C. 6001

DTIC QUALITY INSPECTED 1

OTIS DOES NOT HAVE THIS ITEM

-- 1 - NO NUMBER: 045771
-- 2 - CORPORATE AUTHOR: GENERAL DYNAMICS SAN DIEGO CA CONVAIR DIV
-- 3 - UNCLASSIFIED TITLE: GRAPHITE COMPOSITE TRUSS WELDING AND CAP
-- 4 - SECTION FORMING SUBSYSTEMS. VOLUME 1: EXECUTIVE SUMMARY.
-- 5 - DESCRIPTIVE NOTE: FINAL REPT.,
-- 11 - REPORT DATE: OCT 21, 1980
-- 12 - PAGINATION: 42P
-- 14 - REPORT NUMBER: GDC-ASP-80-007-VOL-1
-- 15 - CONTRACT NUMBER: AASP-15973
-- 18 - MONITOR ACRONYM: NASA
-- 19 - MONITOR SERIES: CR-160933
-- 20 - REPORT CLASSIFICATION: UNCLASSIFIED
-- 22 - LIMITATIONS (ALPHA): APPROVED FOR PUBLIC RELEASE; DISTRIBUTION
-- UNLIMITED. AVAILABILITY: NATIONAL TECHNICAL INFORMATION SERVICE,
-- SPRINGFIELD, VA. 22161. N81-20462.
-- 33 - LIMITATION CODES: 1 24

END OF DISPLAY LIST

((ENTER NEXT COMMAND))

TM: L. Jenkins

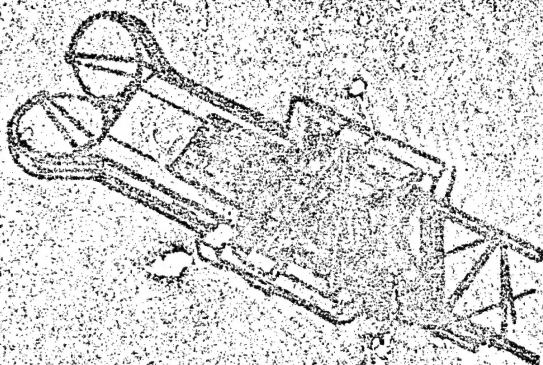
GDC-ASP-80-007

(NASA-CR-160933) GRAPHITE COMPOSITE TRUSS
WELDING AND CAP SECTION FORMING SUBSYSTEMS.
VOLUME 1: EXECUTIVE SUMMARY Final Report
(General Dynamics/Convair) 42 p
HC A03/MF A01

N81-20462

Unclas

CSCL 20K G3/39 19421



GRAPHITE COMPOSITE TRUSS WELDING AND CAP SECTION FORMING SUBSYSTEMS

FINAL REPORT

VOLUME 1 • EXECUTIVE SUMMARY

5. CONTRACT NO. NASA-16073
DRL NO. T-1607
ORD NO. MA-1781
LINE ITEM NO. 3

6 Oct 3, 1980

GENERAL DYNAMICS
Convair Division

Kearny Mesa Plant, P.O. Box 5007
San Diego, California 92162
Advanced Space Programs



GDC-ASP-80-007

**GRAPHITE COMPOSITE TRUSS WELDING
AND CAP SECTION FORMING SUBSYSTEMS**

**FINAL REPORT
VOLUME I + EXECUTIVE SUMMARY**

CONTRACT NO. NAS9-15973
DRL NO. T-1562
DRD NO. MA-179T
LINE ITEM NO. 3

31 October 1980

Submitted to
National Aeronautics and Space Administration
LYNDON B. JOHNSON SPACE CENTER
Houston, Texas 77058

Prepared by
GENERAL DYNAMICS CONVAIR DIVISION
P. O. Box 80847
San Diego, California 92138

FOREWORD

This final report was prepared by General Dynamics Convair Division for NASA-JSC in accordance with Contract NAS9-15973, DRL No. T-1562, DRD No. MA-179, Line Item No. 3. It consists of two volumes: (I) a brief Executive Summary and (II) a comprehensive set of program results.

The principal program results were developed from October 1979 through June 1980 followed by final documentation. Reviews were presented at JSC on 18 March 1980 and 16 July 1980.

During this program, many individuals were involved in providing technical and manufacturing support and assistance. We specifically wish to acknowledge the efforts of the following General Dynamics Convair personnel who significantly contributed to the program.

Structural Design & Analysis	- Lee Browning, Ed Spier, Des Vaughan
Mechanical Design	- John Bodle, Hans Stocker, Bob Clemens
Manufacturing R&D	- Steve Hardy, Gerry Peddie
Materials R&D	- Gay Liskay, Ray Adsit, Mal Campbell, Chuck Horst, Jim Prather, Jose Villa, Carlos Portugal, Mel Wood, Dave Harris, Hector Camacho
Environmental Test	- Don Page, Bill Brunnhoelzl
Experimental Shop	- Don Tibb, Norm Taylor, Dick Renick, Lou Schliffe
Electronics & Instrumentation	- Hugh Arrendale, Ralph Wickwire, Steve Cunningham, Wally Butts, Bob Hayes

The program was managed through Convair's Advanced Space Programs department, directed by R. H. (Russ) Thomas. The program manager was Lee Browning until 21 April 1980. Mr Browning accepted a new position at Convair and was succeeded by his Mechanical and Structural tasks leader, John Bodle. The NASA-JSC COR is Lyle Jenkins of the Spacecraft Design Division, under George Franklin, Chief.

For further information contact:

Lyle M. Jenkins, Code EW4
NASA-JSC
Houston, Texas 77058
(713) 483-2478

John G. Bodle, MZ 21-9504
General Dynamics Convair Division
P.O. Box 80847
San Diego, California 92138
(714) 277-8900, Ext. 2815

TABLE OF CONTENTS

<u>Section</u>		<u>Page</u>
1	INTRODUCTION	1-1
1.1	Scope	1-1
1.2	Program Overview	1-1
1.2.1	Objectives	1-1
1.2.2	Task Summary	1-1
2	PROGRAM RESULTS	2-1
2.1	Cap Forming Technology	2-1
2.1.1	Roller/Heater Geometry	2-1
2.1.2	Drive Rate Effects	2-7
2.2	Ultrasonic Welding Technology	2-9
2.2.1	Weld Test Setup	2-10
2.2.2	Weld Specimens	2-11
2.2.3	Ultrasonic Welding Tests	2-13
2.2.4	Welding Test Results	2-14
2.3	Prototype Truss Segment	2-17
2.3.1	PTS Fabrication	2-17
2.3.2	PTS Test Preparation	2-20
2.3.3	Local Effects	2-21
2.3.4	PTS Test Results	2-28
2.4	Graphite Composite Material	2-32
2.4.1	Forming, Welding, & Truss Material	2-32
2.4.2	Space Environmental Test Material	2-32
3	CONCLUSIONS AND RECOMMENDATIONS	3-1
3.1	Conclusions	3-1
3.2	Recommendations	3-2

INTRODUCTION

1.1 SCOPE

This Executive Summary is one of two volumes comprising the Final Report for the Graphite Composite Truss Welding and Cap Section forming Subsystems Program. Volume II provides the detailed program results.

This section provides a program overview and a top level summary of the program effort.

1.2 PROGRAM OVERVIEW

1.2.1 OBJECTIVES. The overall objective of this development program is to advance the technology required to develop a beam builder which will automatically fabricate long, continuous, lightweight, triangular truss members in space from graphite/thermoplastic composite materials. The primary program objectives are:

- a. Continue the development of forming and welding methods for graphite/thermoplastic (GR/TP) composite material.
- b. Continue GR/TP materials technology development.
- c. Fabricate and structurally test a lightweight triangular truss segment.

1.2.2 TASK SUMMARY. The Space Construction Automated Fabrication Experiment Definition Study (SCAFEDS), was performed under Contract NAS9-15310 by General Dynamics Convair Division for the NASA Lyndon B. Johnson Space Center, in parallel with Convair Independent Research and Development (IRAD). The study produced a concept for an efficient beam builder system for use in on-orbit construction of large space structures. This program's major task groups are structured (as summarized in Figure 1-1) to build on the SCAFEDS design and technology base in the three key areas of forming, ultrasonic welding, and GR/TP composite materials development, test, and evaluation.

The task flow shown in Figure 1-2 indicates the interrelationship between Tasks I and III. After modification and test of Convair's existing bench model cap roll-forming machine, the machine was used to roll-form caps for the prototype test truss and for column test specimens used to test local buckling and torsional instability characteristics.

TOPIC	INPUT	DETAIL TASKS	GROUND RULES	
TASK I CAP FORMING TECHNOLOGY	SCAFEDS PARTS I/II, III	101 ROLLER/HEATER GEOMETRY	• ON EXISTING BENCH MODEL MACHINE	
		102 DRIVE RATE EFFECTS		
TASK III PROTOTYPE TEST TRUSS SEGMENT		301 TRUSS FABRICATION	• GEOMETRY, ELEMENT/JOINT DETAILS, MATERIAL PER SCAFEOS • LENGTH: 4.90m (3 BAYS + STD END CUTOFF) • DIE-FORMED CROSS-MEMBERS	
		302 LOCAL EFFECTS	• STRAIN GAGES & LOAD INTRO FITTINGS PROVIDED • TESTS CONDUCTED AT JSC	
		303 TRUSS TEST PREP/SUPPORT		
		304 MATERIAL	• CONSOLIDATED STRIP FOR TESTING AT LARC: WOVEN SINGLE-PLY GRAPHITE/GLASS; POLYSULFONE RESIN	
TASK II ULTRASONIC WELDING TECHNOLOGY			201 VACUUM EFFECTS	• ON EXISTING COMMERCIAL WELDER
			202 GRAVITATIONAL EFFECTS	• GENERAL DYNAMICS CONVAIR-DEVELOPED HORN/TIPS/SCHEDULES

Figure 1-1. Summary of tasks and ground rules.

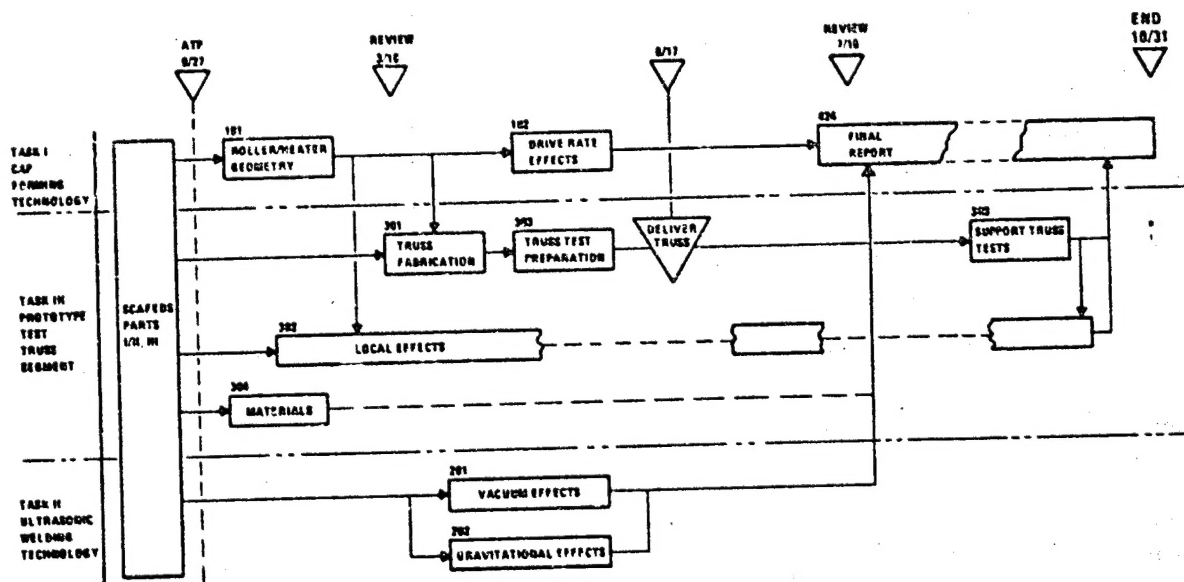


Figure 1-2. Task relationships and flow.

2

PROGRAM RESULTS

2.1 CAP FORMING TECHNOLOGY

A machine for automatically roll-forming graphite/thermoplastic (GR/TP) open-section cap members configured for the SCAFEDS space structure triangular truss and beam builder was demonstrated by Convair in 1978. This early bench model of a beam builder cap forming module showed the need for improvements of the roller and heater arrangements. It had also never been tested at forming rates faster than 1.27 cm/sec (0.5 in./sec). Modification, test, and evaluation tasks were performed in this program to improve performance of, and identify drive rate effects for, the cap forming machine.

2.1.1. ROLLER/HEATER GEOMETRY. The objective of this task was to evaluate and further optimize the operation of Convair's prototype cap forming machine. The goal was to produce "operational quality" cap members, except for conditions caused by lack of sophistication of the machine elements or limited capability to produce uniform, top quality, GR/TP strip material. The factors known to affect cap quality and appearance which could not be resolved within the scope of this task included the following:

- a. Use of surface-contacting thermocouples for temperature control of the heated strips. These thermocouples create scuff marks along the bend zone surfaces.
- b. Lack of a process for continuously coating and consolidating GR/TP resulted in material of nonuniform color, thickness, and flatness due to use of a hot press to compact the strip material in overlapping steps.

The modified cap forming machine is shown in Figure 2-1. The contracted task required redesign, fabrication, assembly, and development testing of the forming section. Each section of the cap forming machine was designed as a separate module to allow each function (i.e., heating, forming, cooling, drive) to be interchangeable with different designs, as required, to evaluate alternative approaches. The forming section was thus replaced without changes to the heating, cooling, and drive sections.

The new forming section used much of the hardware from the original forming section, such as the forming rollers, bearings, shafts, and thermocouples. As shown in Figure 2-2, the original forming section employed numerous quartz lamps beneath and above the strip material. This was to allow flexibility in the adjustments of heaters during early development. The new design employs only four quartz lamp heaters, located beneath the strip, with specially shaped reflectors to direct the infrared heating at the bend zones. External reflector strips are provided along the length of the heated zones to help maintain the temperature of the strips.

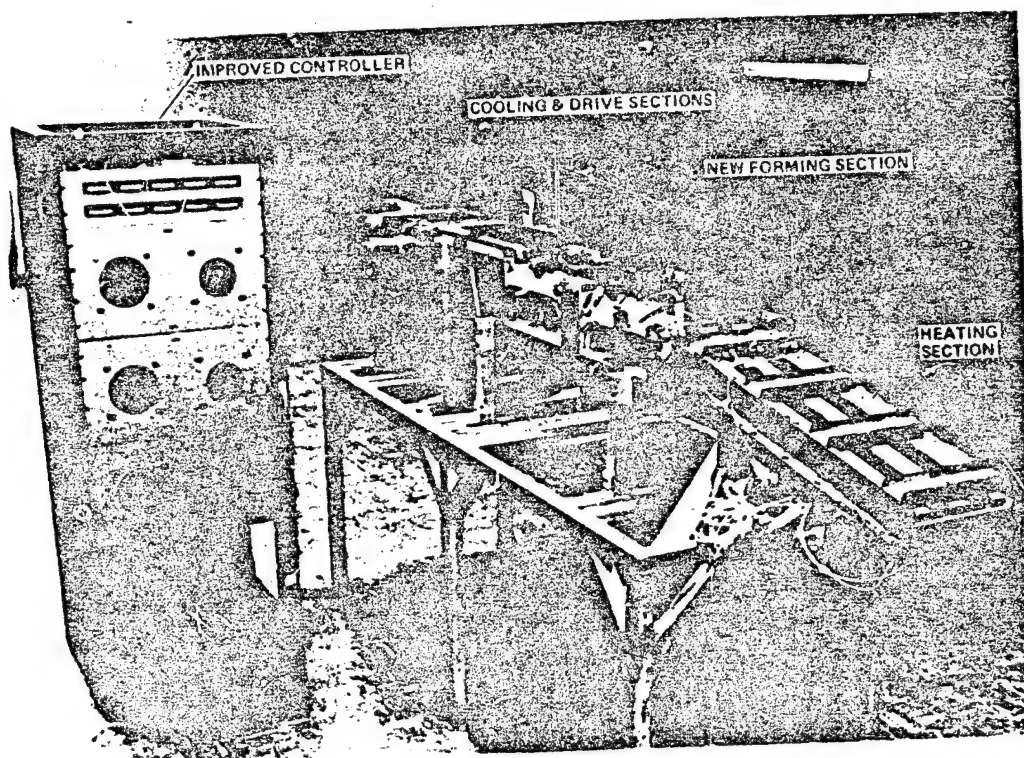
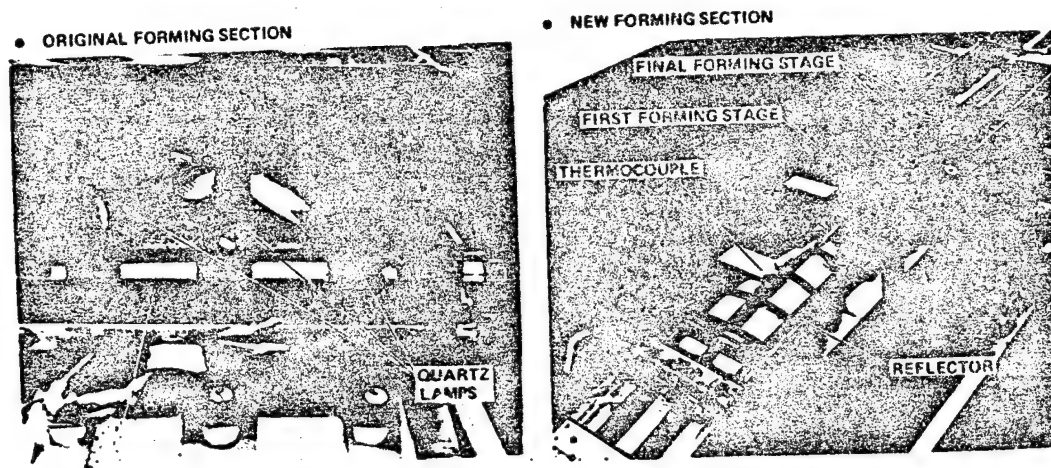


Figure 2-1. Prototype cap forming machine.



- NUMBER OF HEATERS IN FORMING SECTION REDUCED BY 79%
- OVERALL LENGTH INCREASED ~ 15.2 cm

Figure 2-2. Forming section changes.

The distance between the lead-in set of straight rollers and the first forming stage was increased 6.35 cm (2.5 in.) to reduce the strains on the unheated side flats as the strip transitioned from flat to form the 60-degree apex angle. This alleviated the tendency of the center heated strip to fold to a peak just in front of the apex forming rollers, making it difficult to control the width of the heat zone locally in this area during the pause period.

The distance between the first and final forming stage was increased 8.89 cm (3.5 in.) to reduce the strain on the unheated edges of the strip as the 90-degree side bends were formed. The shorter distance had caused the edges to become crimped and wavy during the pause period and had also caused small cracks to occur in the edges. These problems were further alleviated by the addition of teflon guides to support the edges before and after the final forming rollers.

Surface-contacting thermocouples were installed for control and measurement of strip temperatures. Three thermocouples in the forming section connect to three temperature controllers in the control panel which modulate heater power to maintain strip temperatures within a range of 193°C (380°F) to 249°C (480°F).

When the cap forming machine is in operation, as shown in Figure 2-3, the strip is automatically pulled through the process in cycles of 40 seconds run and 30 seconds pause. The controller measures a 58.4 cm (23 in.) stroke for each

run cycle, then stops the motor and closes the water-cooled cooling platens. After 30 seconds, the controller opens the cooling platens and starts the motor. Cyclic feed is a beam builder consideration to allow a pause period during which beam assembly functions are accomplished.

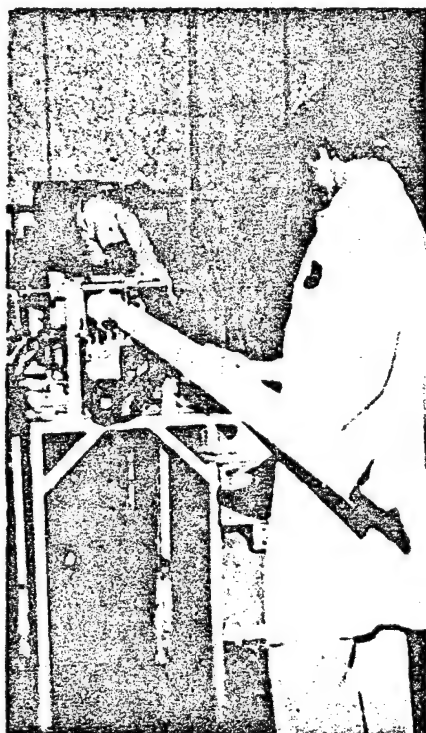


Figure 2-3. Cap forming operations.

The strip material is heated to the forming temperature in the heating section, only along the bend zones, during the 70-second run and pause period. The forming section heaters are required to maintain the forming temperature due to the convective cooling effect of air. Analysis has shown that for operation in the vacuum environment of space, the forming section heaters could be turned off after the initial warm-up, and the heating section heaters would require less energy to heat the material. In-air operation is a consideration, however, because ground test and checkout must be provided for an operational beam builder.

The prototype (bench model) cap forming machine operates in 58.4 cm (23 in.) strokes because the short heating and cooling sections were intentionally included to save cost. For a SCAFE beam builder, the stroke would be 1.439 m (56.46 in.). For a run time of 40 seconds, the maximum strip speed would be approximately 3.8 cm/sec (1.5 in./sec).

A summary of all cap forming tests and operations performed on this program is given in Table 2-1. The first test performed after initial buildup of the forming section resulted in a very poor specimen.

Table 2-1. Summary of cap forming operations.

RUN NO.	DATE	CAP LENGTH	END USE	RESULTS & ACTION
1	14 MAR	2.74m (9 FT)	TEST RUN ONLY	POOR - HEATING ELEMENTS ADJUSTED - SUPPORT GUIDES ADDED
2	9 MAY	2.74m (9 FT)	TEST RUN ONLY	FAIR - MINOR ADJUSTMENTS MADE
3	13 MAY	6.1m (20 FT)	TEST RUN - CRIPPLING SPECIMENS	GOOD - MINOR IRREGULARITIES - INSULATED SUPPORT BRACKETS
4	14 MAY		COLUMN TEST SPECIMEN	GOOD
5	14 MAY		PROTOTYPE TRUSS CAP	GOOD
6	15 MAY		PROTOTYPE TRUSS CAP	GOOD
7	15 MAY	6.1m (20 FT)	PROTOTYPE TRUSS CAP	GOOD

TOTAL 36m (118 FT)

A substantial number of modifications were made to improve performance. Heating profiles were tested to pinpoint problem areas requiring adjustments and modifications. More edge guides and side support guides were added to prevent waviness of the free edges and wrinkling along the bend zones.

The second test showed a marked improvement in the uniformity of the finished cap. Some further adjustment of guides were required to correct minor creases along the bend zones.

The third test specimen was the first 6.1 m (20 ft) specimen to be run. It was generally uniform in cross section, with some minor irregularities which will be discussed later. One set of support brackets in the forming section was wrapped with fiberglass because it was suspected of creating a local hot spot in the edges.

It was decided at this point to proceed with the forming of the specimens for column test and the caps for the prototype test truss. It was recognized that further efforts to eliminate minor irregularities would require more time, money, and material than were available. It should be noted, however, that the causes of every irregularity observed were eventually identified, and none were found that could not be remedied by either improving the material processing techniques or making some minor changes in the forming section reflectors.

• PROTOTYPE TRUSS CAPS

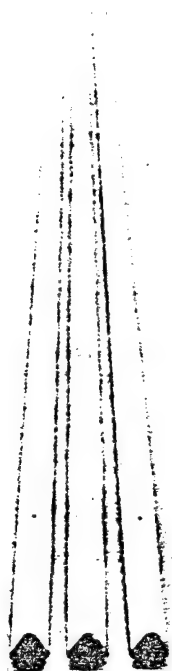
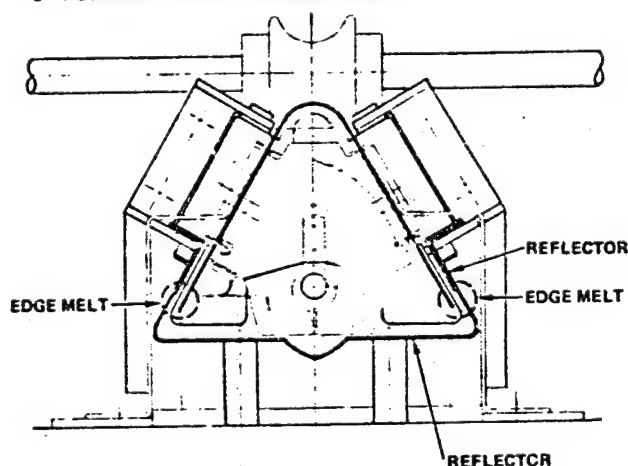


Figure 2-4. Cap forming results.

The last four caps were run in sequence without further change or adjustment of the cap forming machine. The results achieved on the prototype truss caps are shown in Figure 2-4. There were two very noticeable irregularities in the finished caps. The first was a local edge deformation, shown in Figure 2-5, which occurred at regular stroke length intervals. This suggested a local hot spot somewhere in the forming section that was radiating enough heat on the edges to cause them to soften and become deformed. Post-test analysis of this problem identified a 2.54 cm (1.0 in.) wide reflector support just forward of the first forming stage as the cause. This support was attached directly to both an internal and an external reflector, which caused it to get hot enough to melt the cap edges locally.

• FORMING SECTION TROUBLE SPOT



• LOCAL EDGE DEFORMATION

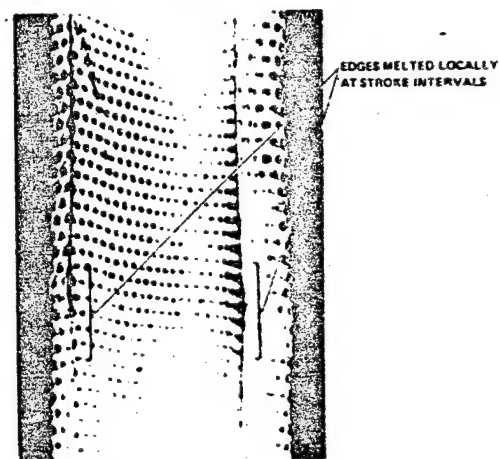


Figure 2-5. Irregularities due to heating.

The second noticeable irregularity was that all of the formed caps exhibited a relatively constant curvature in the plane of symmetry as seen in Figure 2-6. A careful check of the alignment of the axially linear element in the cap forming machine failed to identify anything that would account for this curvature.

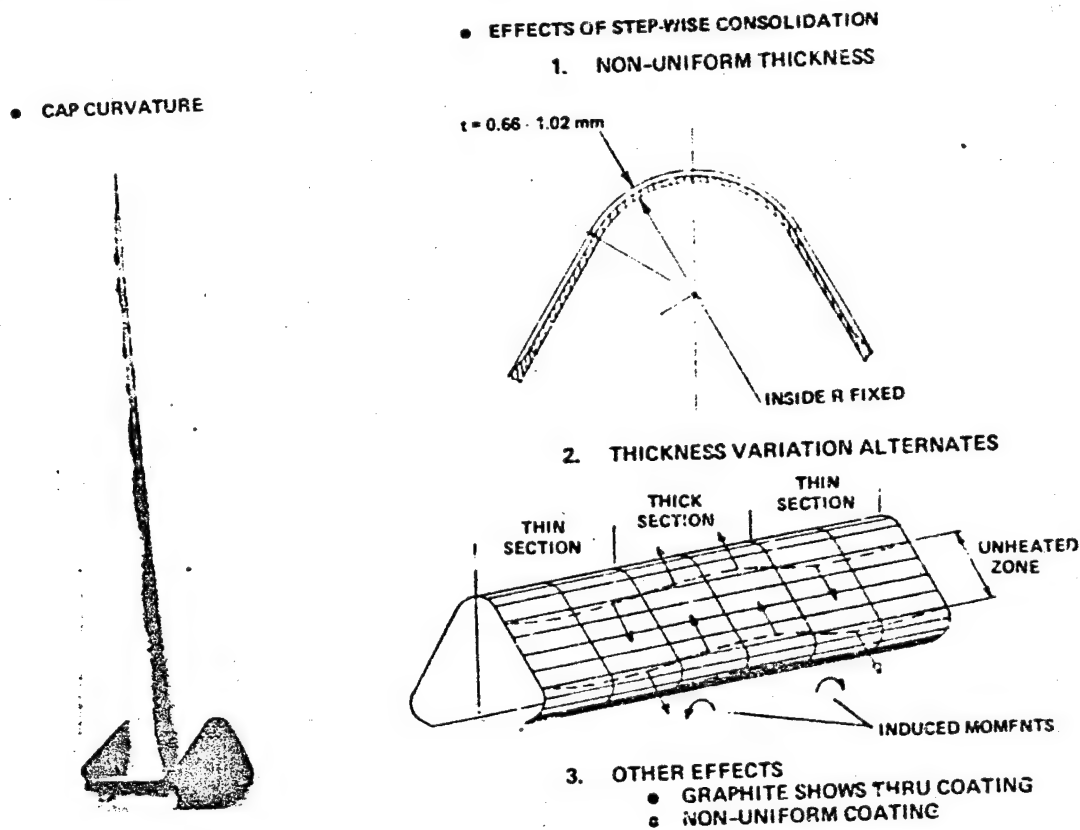


Figure 2-6. Irregularities due to material processing limitations.

After general inspection of the strip material, it was theorized that the curvature may be induced by nonuniformity of the material thickness. Step-wise compaction of the strip results in alternately varying material thickness over its entire length. The effect of the alternating thickness variation on cap shape is illustrated in Figure 2-6. The inside geometry of the cap section is fixed by the forming rollers and cooling platens and the arc perimeters of the outside radii change with thickness. This alternating shortening and lengthening of the arc perimeters causes stresses along the boundaries of the unheated side flats and edges, which induce moments along the length of the cap. Since the open section allows the cap to distort under the influence of these stresses, the cap will tend to bow in the direction of least resistance.

The curvature of the caps did not affect truss assembly because it took very little force to straighten the caps out on the truss welding fixture. The curvature did, however, introduce an unexpected variable to the cap crippling and column test specimens.

2.1.2 DRIVE RATE EFFECTS. An experiment was performed to determine the effects of driving the strip material through the forming section at increased rates of speed. This section describes the changes made to the drive section to perform this experiment, the test method, and results of testing.

The original drive section contained molded elastomeric drive rollers driven in unison by a 1/50 horsepower DC motor through a gear train. A resolver wheel on the motor shaft created pulses from an optoelectronic interrupter which were input to a cap displacement controller. This provided a resolution of approximately 96 pulses per inch of cap travel. By setting the desired run length on the control panel, the cap displacement controller stopped the drive motor when the required pulse count accumulated. This measurement technique was not very accurate because the elastomeric rollers introduced an error in the actual-versus-indicated cap displacement. To improve accuracy of cap displacement measurement, an optical shaft encoder was installed over the cap member. To permit driving the cap at increased speeds, the drive motor and gear ratio were changed. These drive section modifications are shown in Figure 2-7.

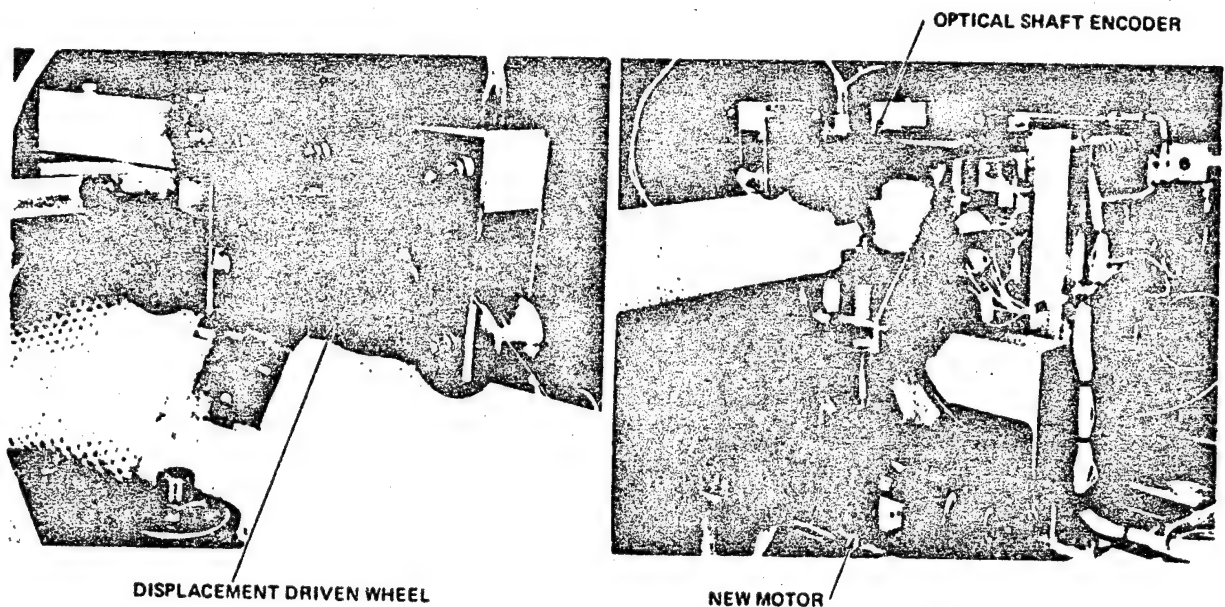


Figure 2-7. Drive section modifications.

The optical shaft encoder pulses output signals at the rate of 100 pulses per inch of cap travel in response to the rotation of the displacement drive wheel. This technique improved the accuracy of cap displacement measurement by an order of magnitude.

The new drive motor is a 1/15 horsepower DC shunt-wound, which is driven open-loop, with no velocity feedback or control. The motor thus tends to slow down under increased load, which results in variable velocity during test runs.

For a beam-builder system, a more sophisticated drive control would be required to ensure uniform displacement of caps during the run phase, and highly accurate displacement control of each beam cap to ensure straightness of long beams.

The drive rate effects test was run using a 6.1 m (20 ft) length of strip material. This allowed eight different speeds to be run. The speeds were selected between the minimum speed of 3.8 cm/sec (1.50 in./sec), which is the baseline speed for the SCAFEDS beam building, and 31.8 cm/sec (12.5 in./sec) which is the speed derived for the Solar Power Satellite growth version of the beam builder.

Because the pause time required at the maximum speed was 68 seconds, all test runs were made using the 68 second pause time. This eliminated pause time as a variable from run-to-run.

The drive rate effects identified during this experiment are summarized in Figure 2-8. There were no speed-related effects noted until the velocity reached 10.2-12.7 cm/sec (4.0-5.0 in./sec). The irregularities in the cap section at the lower speeds were all related to the larger-than-normal pause time and were all heating or cooling effects.

This one brief test indicated that careful attention will be required in the design of forming section heaters for the beam builder cap forming module to achieve uniform heating. This basic forming process is compatible with drive speeds required for near-term beam builders and can be adapted to higher drive speeds through further development.

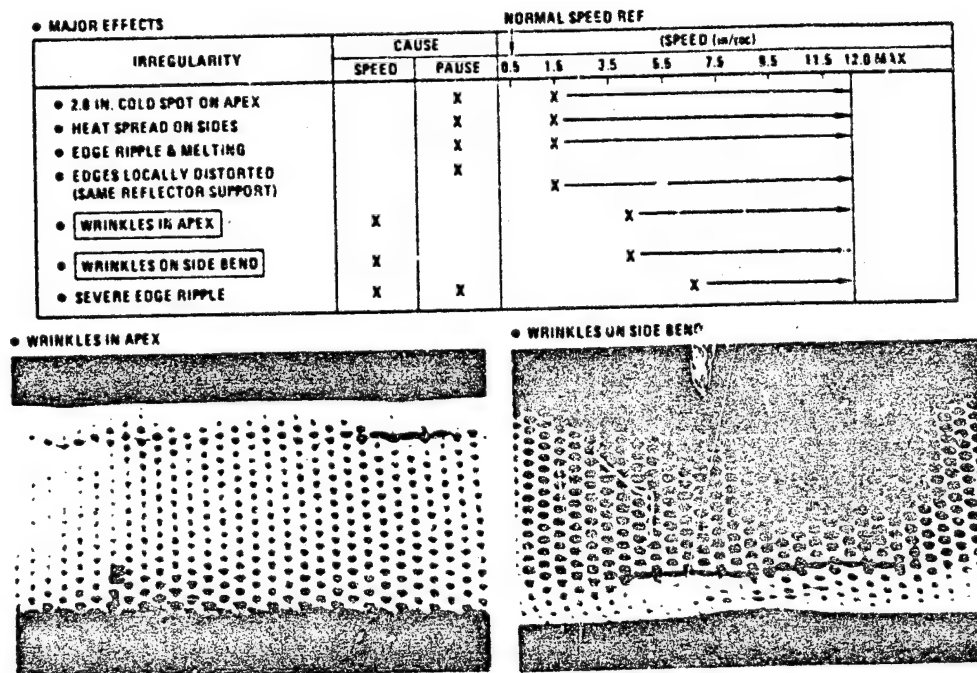


Figure 2-8. Drive rate effects summary.

2.2 ULTRASONIC WELDING TECHNOLOGY

Ultrasonic welding of composite materials has been developed extensively in the environment of air and gravity. Prior to final selection of this method for joining structural members together in the environment of space, experiments to investigate the effects of gravity and vacuum on the composite material and welding apparatus were required.

The objectives of the ultrasonic welding task were to investigate and evaluate the following:

- a. Solidification of ultrasonic welds by investigating weld heat buildup and dissipation during the welding operation in a thermal-vacuum simulation.
- b. Ultrasonic weld flow in a zero-g environment by determining the effect of gravity on the molten weld.

Investigation of the effects of gravity and vacuum on the ultrasonic welding process was conducted by instrumenting an off-the-shelf Branson Sonic Power Co. Model 4120 ultrasonic welder to operate in a vacuum chamber and in three different angles to gravity. The experimental procedure, illustrated in block diagram form in Figure 2-9, was developed to identify any vacuum, gravitational, or combined effects on the welder, material, or final weld strength.

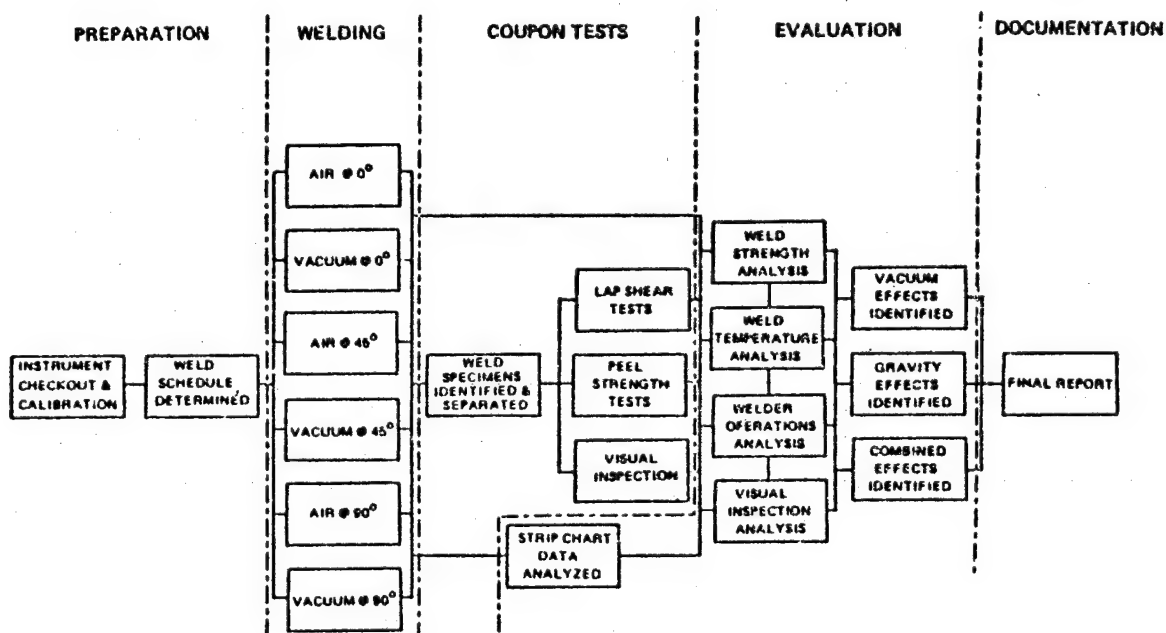


Figure 2-9. Welding task approach.

2.2.1 WELD TEST SETUP. The test setup, illustrated in Figure 2-10, allowed for control and monitoring of the welder from outside the vacuum chamber.

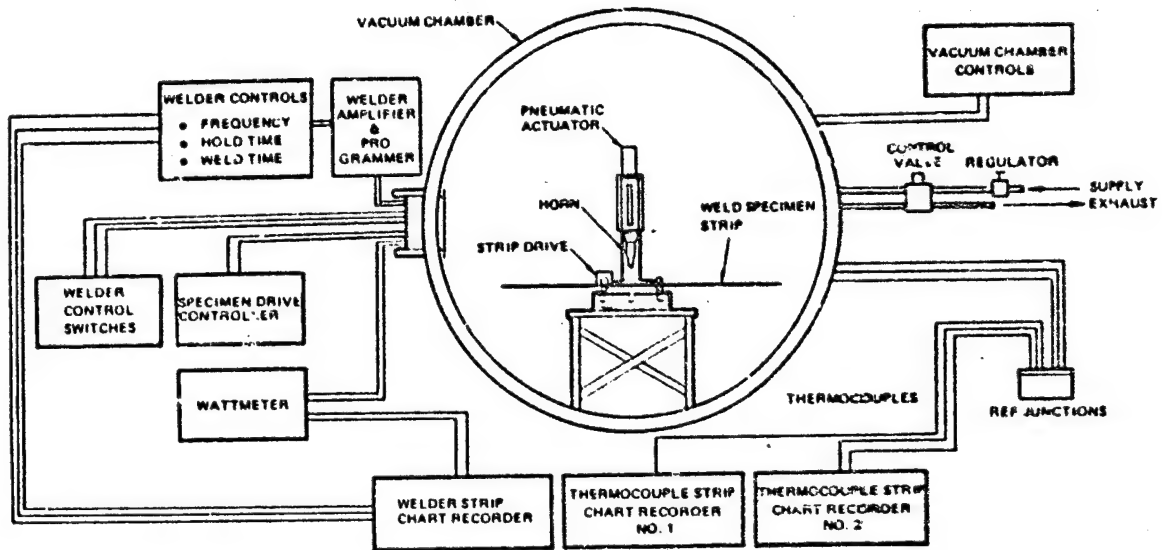


Figure 2-10. Welder instrumentation and controls diagram.

For consistent weld schedules, the weld time, hold time, weld pressure, and frequency must be accurately controlled. Timing control to an accuracy of ± 0.02 second was accomplished by using a special controller to control weld time and hold time.

Weld pressure was controlled by a pneumatic regulator outside the chamber in the air pressure supply to the welder pneumatic actuator. Air pressure to the actuator and exhaust from the actuator was conducted by tubing through a solenoid control valve outside the chamber. Weld frequency was monitored by a digital counter.

Two 8-channel rapid-read strip chart recorders were used to monitor the operation of the welder, temperature of the welder, and temperature of specimens for heat flow tests. One recorder monitored weld power, horn down time, weld time, and temperatures of the piezoelectric transducer, booster, horn mid-point (area of maximum strain), and weld tip. The other recorder was used for temperature sensing eight places on the welded specimens to determine heat flow characteristics.

Weld testing was performed with a 1.27 cm ($\frac{1}{2}$ in.) diameter course knurled tip (total surface area approximately 2.53 cm² (0.393 in.²) attached to an ultrasonic weld horn with a gain of 6.6. Total tip motion with a 1:1 gain booster is 0.01257 cm (0.00495 in.).

Previous weld tests conducted using the GR/TP composite material had shown that the weld strength will reach a peak as a function of energy input. As more energy is input to the bond area, degradation of the material eventually begins to weaken the weld. The peak weld strength occurred within a range of energy between 310 J/cm² and 496 J/cm² of weld area. It was assumed that the identification of a relatively minor weld strength degradation caused by gravity direction or vacuum around the weld area might not be apparent if a peak strength weld schedule were used. Consequently, the weld schedule selected was approximately 155 J/cm² so that small deviations in welder efficiency, resin flow, material uniformity, temperature flow, etc. would cause an easily identified change in weld strength.

The weld schedule used for all weld tests specimens was as follows:

- a. Weld Time - 0.7 second
- b. Hold Time - 1.0 second
- c. Pneumatic Pressure - 27.6 N/cm² (40 psig)

2.2.2 WELD SPECIMENS. To allow a series of welds to be performed inside the vacuum chamber, two 122 cm x 6.35 cm strips of GR/TP composite material were joined together as shown in Figure 2-11 with a 2.54 cm overlap. The strips were incrementally moved by a remotely controlled motor drive system as shown in Figure 2-12. Each weld strip was baked at 533K (500F) for 3 hours then vacuum bagged and baked for 18 hours at 389K (350F) to remove moisture and volatiles which can effect weld strength and vacuum chamber pressures. The weld test specimens are summarized in Table 2-2. The weld strips were designed to accommodate 35 to 38 weld specimens of the number and type indicated. Each weld was identified as to number, environment, and gravity orientation.

Table 2-2. Weld test specimen requirements.

Usage	Air			Vacuum		
	0°	45°	90°	0°	45°	90°
Preliminary	20	5	5	5	5	5
Lap Shear	40	25	25	25	25	25
Peel	5	5	5	5	5	5
Visual Insp.	5	5	5	5	5	5
Temperature	3			3		
Total	58	35	35	35	35	35

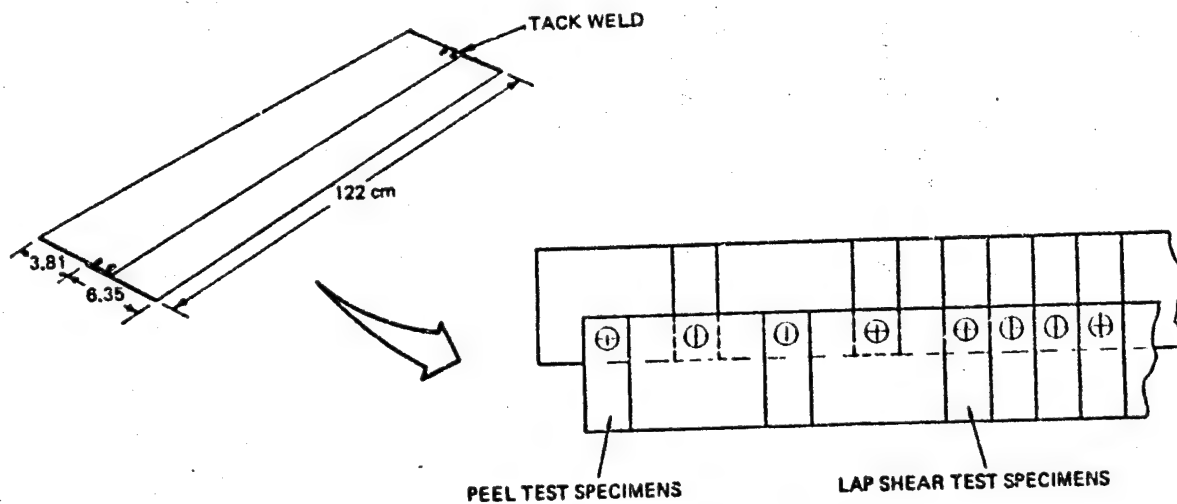


Figure 2-11. GR/TP weld test strip configuration.

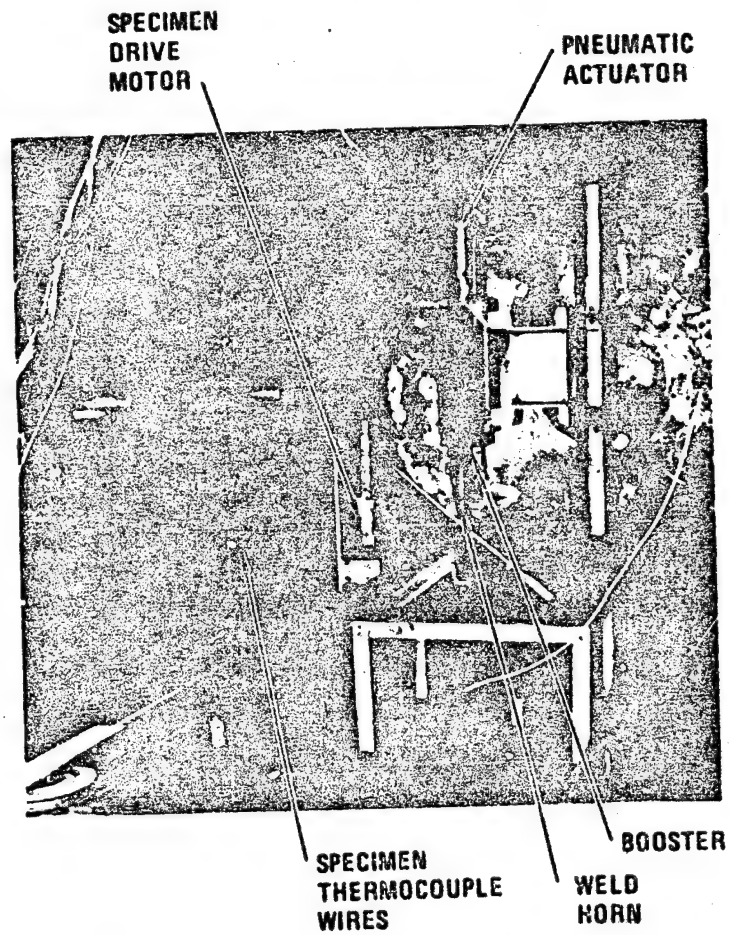


Figure 2-12. Vacuum chamber 0° setup.

2.2.3 ULTRASONIC WELDING TESTS. Following the checkout and calibration of all instruments, a preliminary test of the total system was conducted. Twenty-weld test specimens were successfully welded in air with all instruments operational, the welder oriented in the 0-degree configuration (Figure 2-12). The welder amplifiers and programming module were inside the chamber.

The initial attempt to weld in vacuum resulted in erratic and generally very low power to the transducer; the weld and hold time were inconsistent; and the frequency was erratic. As a result, there was no weld or melt in the composite material. Trouble shooting of the electronics and actuator were inconclusive. Factory checkout and repair of the amplifiers and programmer, and replacement of the transducer had no effect. Removal of amplifiers from the vacuum chamber was not successful due to wiring problems between the amplifiers and the programmer inside the chamber. Removal of all electronics from the chamber resulted in normal timing and frequency, but welding was still intermittent. Finally, removal of an aluminum label over the top of the transducer to insure proper venting of internal air pressure during pump-down resulted in normal welder operation in vacuum. It was concluded that when the chamber was pumped down, some of the electronic components in the amplifiers, programming module, and transducer malfunctioned, probably due to internal corona effects causing electrical short circuiting.

The vacuum and gravity effects welding tests were conducted in the sequence shown in Table 2-3. Vacuum pressures ranged from 4.8×10^{-3} N/m² (3.6×10^{-5} Torr) maximum to 1.07×10^{-3} N/m² (0.8×10^{-5} Torr). A separate test strip was installed for each run. Welder orientation was changed by tilting the apparatus as shown in Figure 2-13. No changes were made in weld schedule and no adjustments made to the welding apparatus except for periodic tuning of the weld stack.

Table 2-3. Weld test sequence.

Run No.	Environment	Welder Orientation
1	Air	0°
2	Vacuum	0°
3	Air	90°
4	Vacuum	90°
5	Air	45°
6	Vacuum	45°

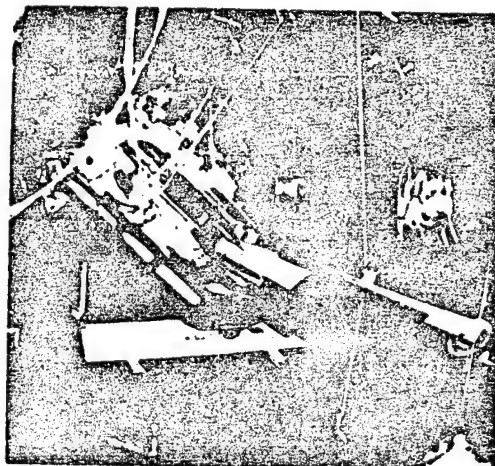


Figure 2-13. Vacuum chamber 45° setup.

2.2.4 WELDING TEST RESULTS. Upon completion of each weld test, the weld strip was removed from the drive mechanism and the individual welds were cut out and separated into the test groups described in Table 2-2. Table 2-4 summarizes the lap shear and peel test data. Air and vacuum welds made at 90 degrees were notably lowest in strength and had the lowest ratio of success. A possible explanation for the lower weld strength at the 90-degree angle is that since the horn is slender and tapered from 6.35 cm at the top to 1.27 cm at the weld tip, some of the weld energy may be converted into transverse motion due to cantilevered vibration of the horn. This condition is a gravity effect on weld strength which would not exist in a zero-g earth-orbit environment. In gravity, this whipping condition can be compensated for by increasing weld pressure and/or time. A horn of greater cross section, such as that designed for the truss welder, would have less tendency to whip.

Table 2-4. Summary of lap shear and peel tests.

Welder Angle	In-Air						In-Vacuum					
	Lap Shear			Peel			Lap Shear			Peel		
	n	(N)		n	(N)		n	(N)		n	(N)	
		\bar{P}_L	$\pm\sigma$		\bar{P}_p	$\pm\sigma$		\bar{P}_L	$\pm\sigma$		\bar{P}_p	$\pm\sigma$
0°	25	814.0	333.6	3	24.9	17.3	18	582.7	213.5	0	0	—
45°	24	649.4	155.7	5	20.0	10.2	25	796.2	253.5	5	16.0	8.5
90°	8	431.5	155.7	0	0	—	16	471.5	124.6	4	8.9	7.1

All weld specimens were examined for resin flow, resin melt, and general appearance differences which might result from welding in vacuum or from gravitational effects. There was no difference in tip penetration or flow on the surface of the welds which could be related to the gravitational or ambient conditions under which the weld was made. Flow characteristics of thermoplastic in the faying surfaces were very similar. The only variations were caused by differences in material resin content and thickness along the material strips.

Thermocouples attached to the weld head during the welding experiments were continually monitored to determine the cooling and heating effects of the lack of or presence of air. Figure 2-14 illustrates the weld head thermocouple locations. Table 2-5 shows the maximum change in temperatures from start of weld sequence to completion of the last test weld using the prescribed weld schedule with 80-second intervals between welds. Weld tip operating temperature data was lost during test due to separation of the thermocouple and fractional heating interaction between the thermocouple and the weld tip. It is assumed that the weld tip temperatures after 80 seconds of cooling approached the temperature of the horn. The maximum temperature changes occurred in the horn in vacuum. This change was not significant; however, the total welding time was not long enough to allow the weld horn to reach an equilibrium temperature.

Table 2-5. Weld head heating effects.

Angle	Environment	$\Delta T (^{\circ}F)$			
		Tip**	Horn	Bstr	Trans
0°	Air	-	3	3	3
45°		-	2	2	2
90°		-	9	1	1
0°	Vacuum	-	21	6	4
45°		-	14	4	5
90°		-	23	9	8

*Rise in preweld temp in ~50 min (35 weld cycles)

**Tip thermocouple separated

Figure 2-14 illustrates the maximum temperature change characteristics of each weld head component during weld cycles in air and in vacuum. In air, the horn temperature increased approximately 35°F during weld, but returned to near ambient within 10 seconds. In-vacuum temperature changes were similar to changes in air, but with slower decay rates apparently due to the lack of convective cooling. In both air and vacuum welds, the maximum change in temperature occurred at the 90-degree weld direction, which suggests increased heating due to bending strain in the horn.

• THERMOCOUPLE LOCATIONS

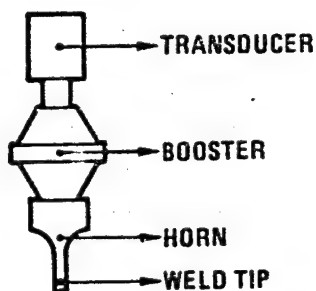


Figure 2-15 illustrates the thermocouple locations and material fiber orientation on the weld strips for the 0-degree air and vacuum tests, and shows the temperature changes that occurred at thermocouples 7 and 10 in air and in vacuum. Results of these tests showed only minor heating external to the weld area in the direction of the glass fibers. The peak temperatures at thermo-

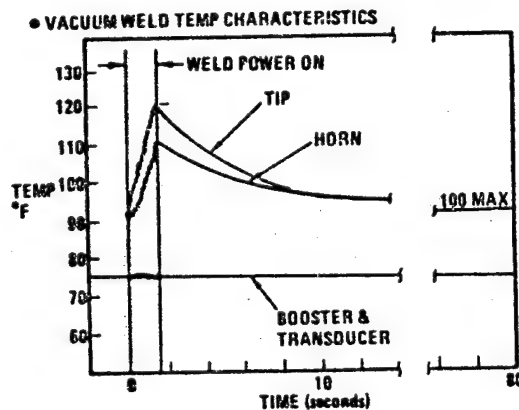
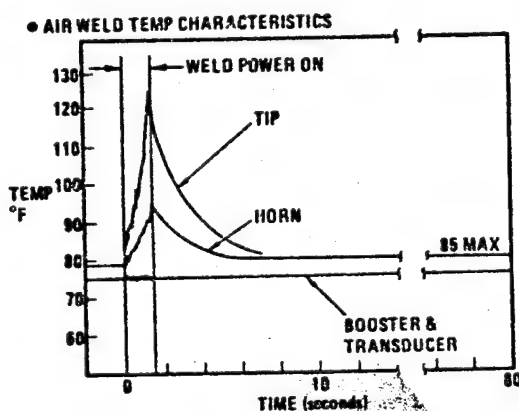


Figure 2-14. Weld head temperature characteristics in air and in vacuum.

couples 6, 9, and 12 (nearest the weld) showed an increase of 10 to 20°F. Average temperatures at 5, 6, 8, 9, 11, and 12 during the welding of T1, T2, and T3 were 83°F in air and 105°F in vacuum.

• WELD STRIP & THERMOCOUPLES

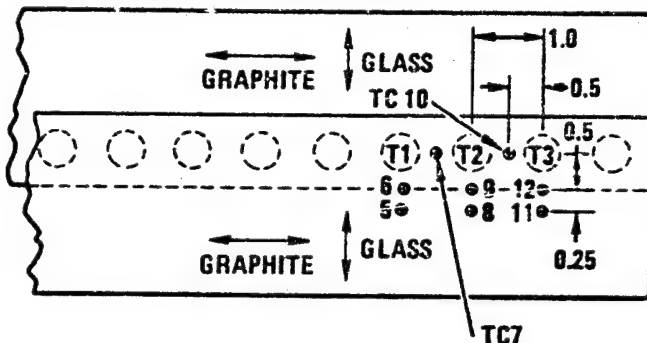


Figure 2-15. Thermocouple locations for air and vacuum temperature flow tests.

Figure 2-16 shows that the maximum peak temperatures occurred along the graphite direction nearest the weld. The differences in peak temperatures between TC7 and TC10 are attributable to inaccuracy in positioning the strip under the weld tip.

During preliminary air weld tests, it was found that two distinct power curves were being generated. On further analysis of the material, it was determined that the power curve profiles were a result of the GR/TP surface

roughness on the faying surfaces. Figure 2-17 shows a typical power curve for GR/TP with smooth faying surfaces and the power curve caused by rough faying surfaces.

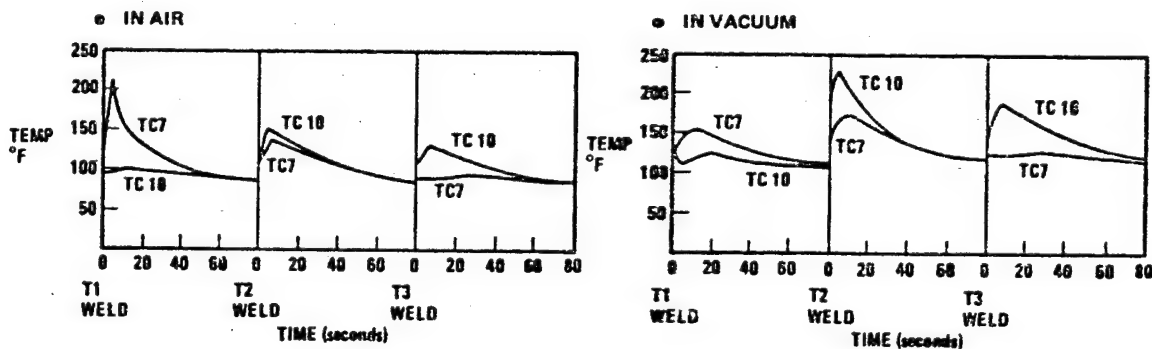


Figure 2-16. Weld specimen heat flow characteristics in air and in vacuum.

The total area under these curves is similar, indicating nearly equal energy (watt-seconds-joules) input to each weld. Weld strength was also similar, as would be expected with equal energy input, time, and pressure.

The third power curve, shown in Figure 2-17, was also created when welder efficiency was affected by gravity or material variations (thickness, resin content, or roughness) and the resulting weld strength was significantly lower.

These results support the beam builder welder concept, wherein weld energy would be electronically monitored and controlled to insure optimum weld quality.

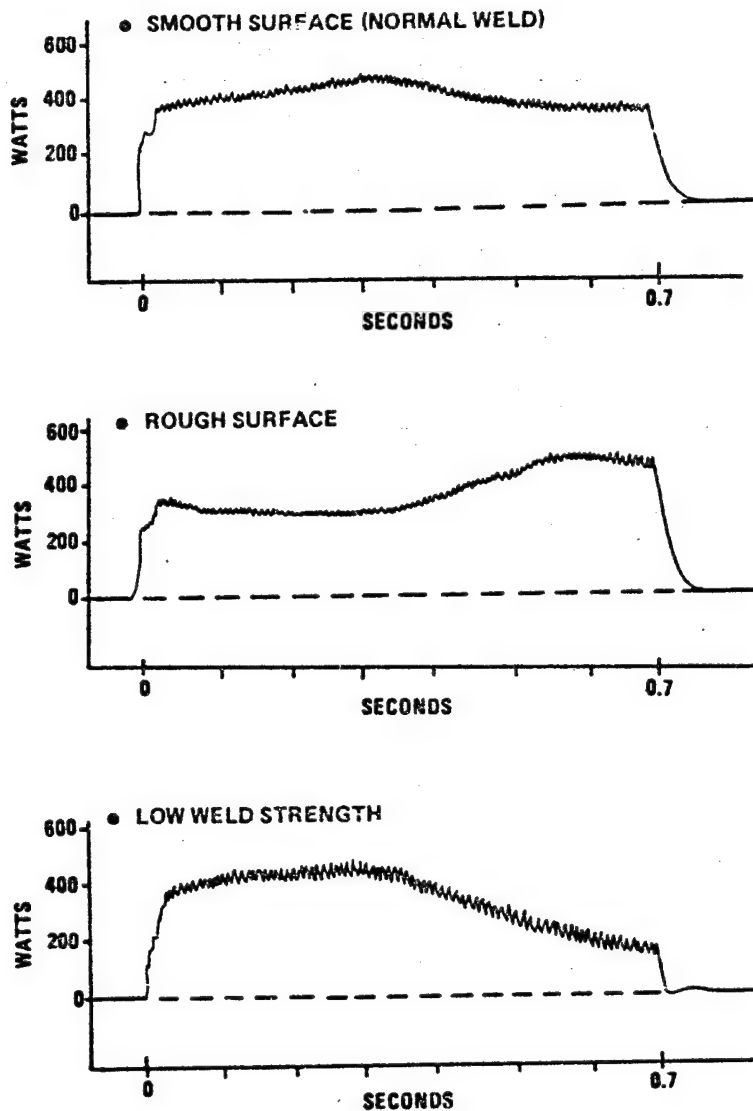


Figure 2-17. Power curve variations.

were automatically roll-formed from flat preprocessed composite strips using the roll forming machine which had been modified as described in Subsection 2.1.1.

The crossmembers were manufactured from the same composite material as the caps. Each crossmember was individually formed using a die form tool. This is in keeping with the SCAFEDS beam builder design, which uses preformed crossmembers.

2.3 PROTOTYPE TRUSS SEGMENT

The requirement to fabricate, test, and evaluate a three-bay prototype triangular truss segment which conformed to the design developed for the SCAFEDS comprised three major tasks: (1) truss fabrication for the manufacture of the Prototype Test Truss (PTS); (2) truss test preparation and support to prepare test plans, install strain gages, and load introduction fittings, and to provide technical support to NASA/JSC during test; and (3) local effects analyses and tests to characterize cap crippling, buckling, and torsional instability effects for comparison with PTS test results.

2.3.1 PTS FABRICATION.

The PTS configuration is shown in Figure 2-18. The cap members for the PTS were manufactured from graphite/glass/polysulfone, single-ply woven composite material described in Subsection 2.4.1. All three caps

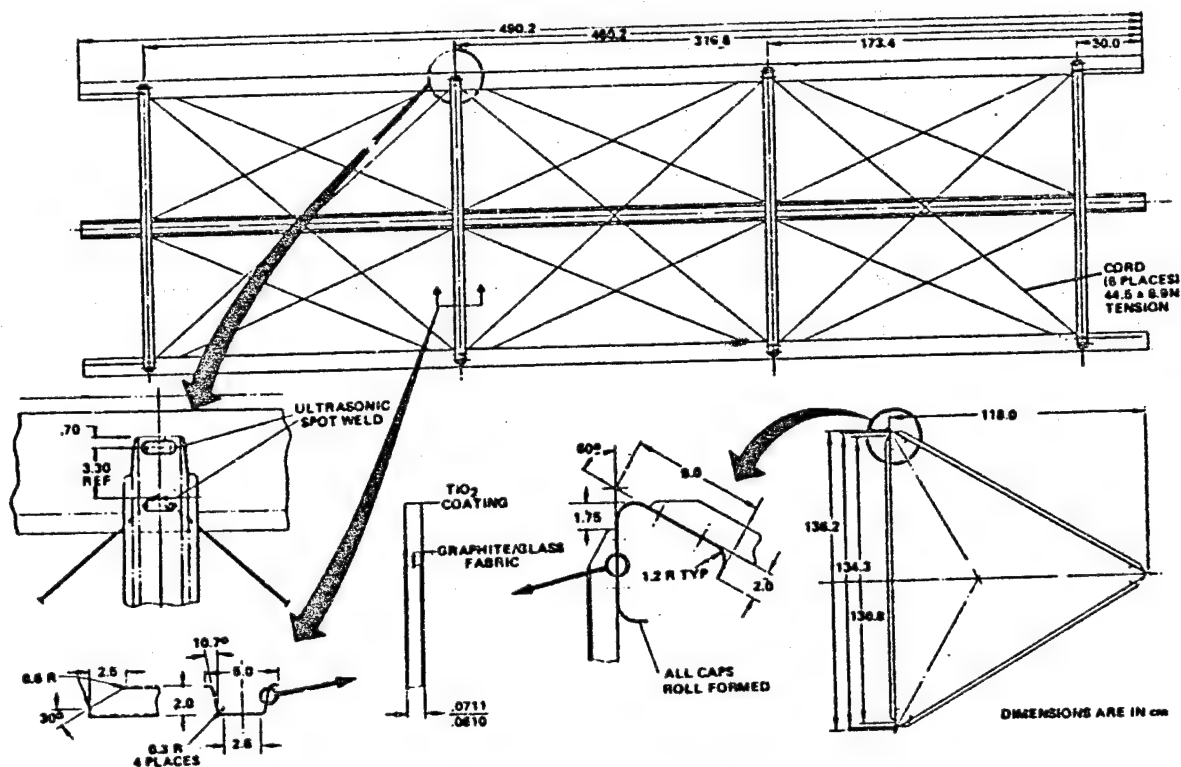


Figure 2-18. Prototype truss segment configuration.

The diagonal cord material is a 20-end S-glass roving impregnated with P-1700 polysulfone resin and manufactured by U.S. Polymeric. The cord was consolidated to a circular cross section (to improve its strength properties) by immersing it in a polysulfone and solvent bath and pulling it through a circular die.

To assure dimensional accuracy and minimize assembly time for the PTS, a rigid welding and assembly fixture was designed and built. The fixture consisted of a steel pipe with twelve arms attached. Each arm supported an aluminum anvil shaped to fit the internal geometry of the caps. The fixture was supported on each end by tooling stands. The pipe rested on steel rollers attached to the end stands. This allowed the entire fixture to be rotated to facilitate truss assembly.

The steps followed in assembling the PTS are illustrated in Figure 2-19. After trimming the caps to length, they were placed on the tool and the cross-member stations were measured and marked off on each cap. Pierce-pin locator holes were then located on each cap at each weld location. With the caps aligned with their ends in-plane and the crossmember centerline stations centered on the weld anvils, each locator hole was predrilled through the cap to a depth of 1.3 cm into the anvil.

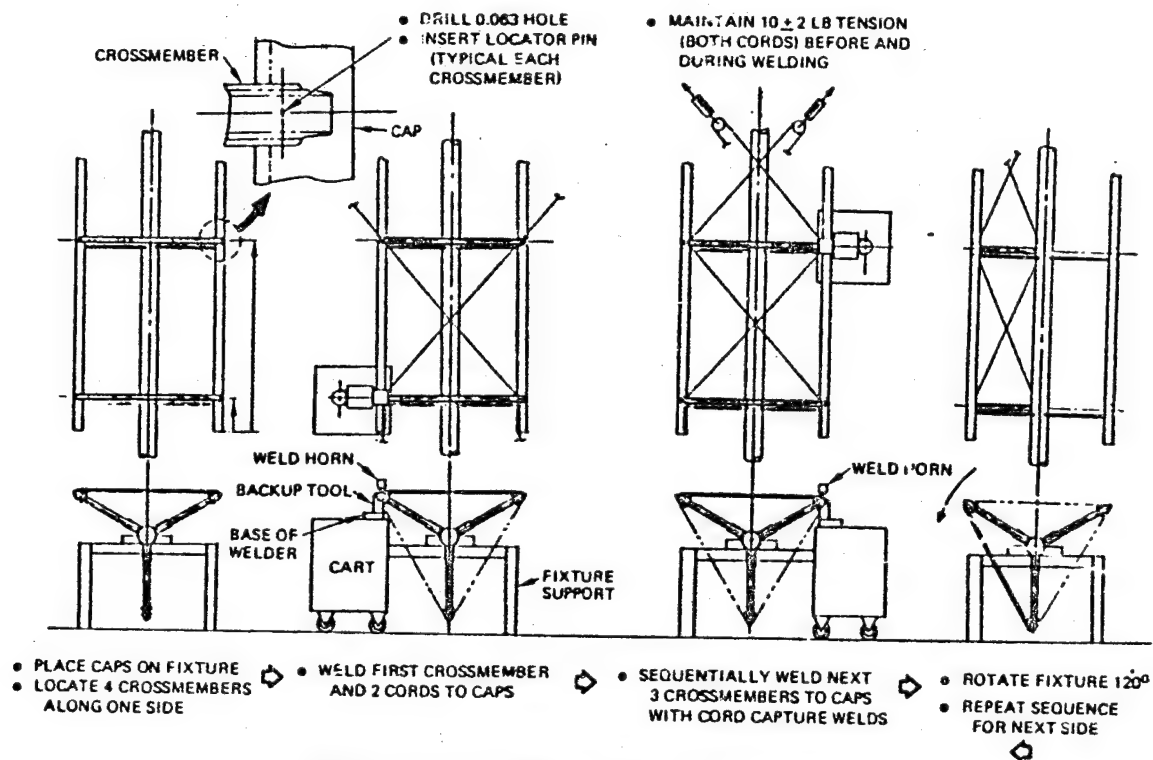


Figure 2-19. Truss fabrication plan.

The ultrasonic welder was set up to perform truss welding, as shown in Figure 2-20. A standard commercial welder (Branson Model 8600) was placed on a table equipped to raise and lower the welder with a hydraulic lift mechanism and to move it from station to station on wheels.

The Convair-developed multi-spot weld horn is equipped with a short 1.6 mm (0.063 in.) diameter piercing pin. This pin is provided as part of the beam builder operating concept to act as a fulcrum over which the diagonal cord is wrapped. The weld cycle attaches the crossmember to the cap and captures the cord within the weld zone. For assembly of the PTS, all crossmembers were prepositioned on the predrilled pierce-pin holes by locating pins inserted in each hole. After positioning the welder, the locating pin was removed and the weld horn manually lowered to insert the pierce-pin the drilled hole. The cord was positioned against the pin and between the cap and crossmember. For the first crossmember, the cords were aligned but not tensioned, since it was only necessary to capture the cords on this first weld. On subsequent welds, the cords were first aligned against the pierce-pin, pulled in tension using a fish scale, then wrapped over the pierce-pin while maintaining tension until the cord just touched the locating pin at the next crossmember station. Weld pressure was then applied to clamp the cord between the crossmember and cap and maintain tension during the weld sequence. Figure 2-21 shows a typical finished weld.

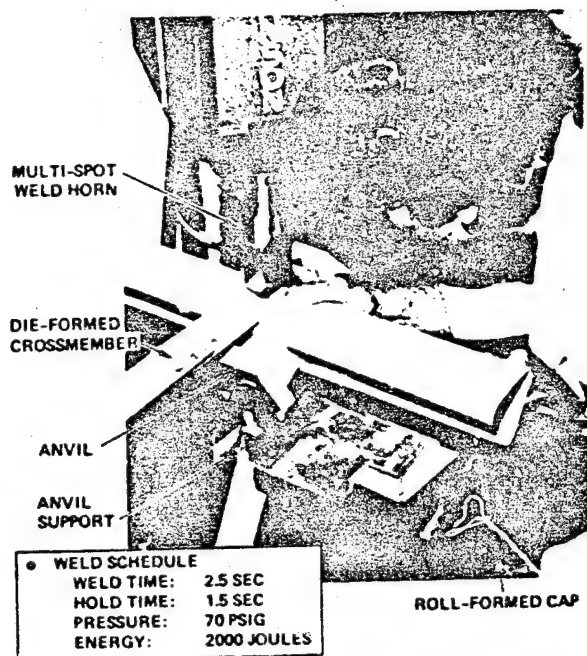


Figure 2-20. Truss ultrasonic welder.

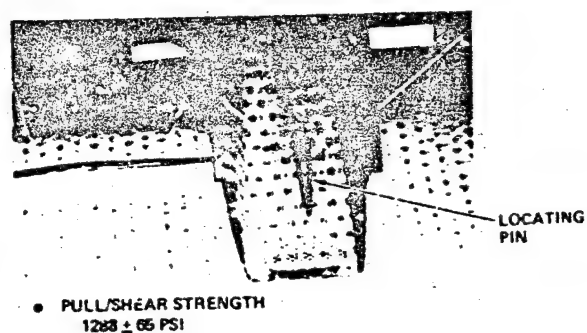


Figure 2-21. Finished weld joint.

2.3.2 PTS TEST PREPARATION. After the PTS was assembled, the end load introduction fittings were positioned and installed with the truss still in the assembly fixture. The load introduction fittings consisted of aluminum form blocks inserted into the end of each cap and braced with aluminum angles as shown in Figure 2-22.

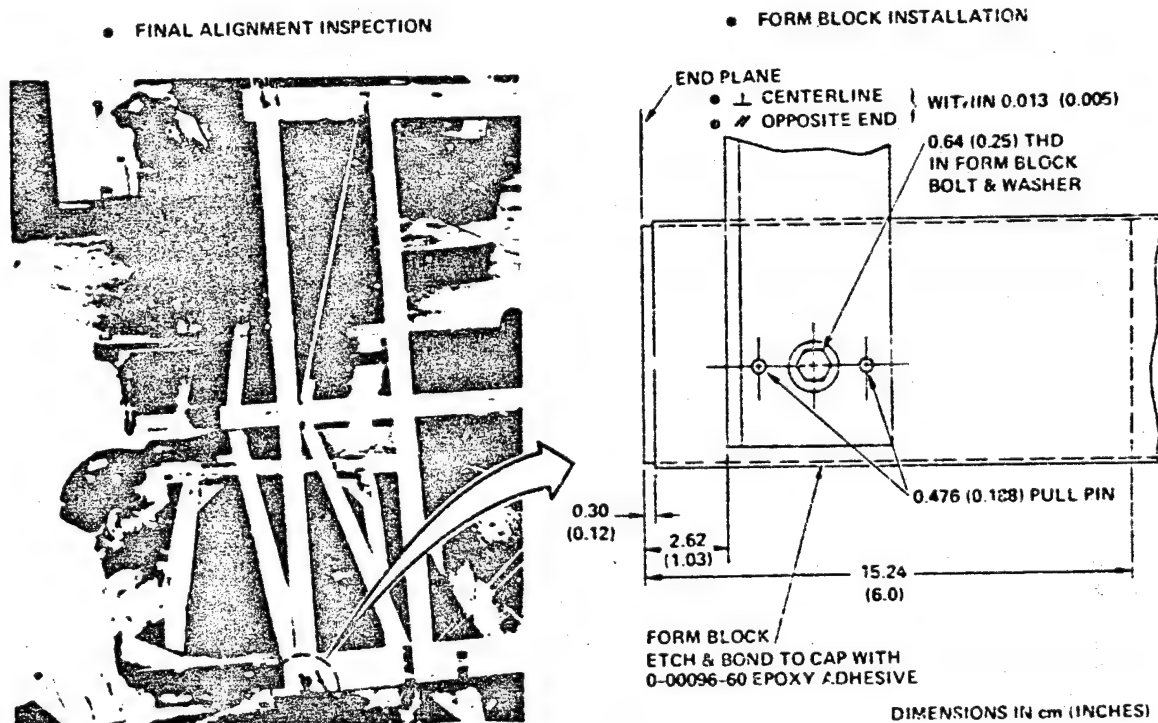


Figure 2-22. Truss load introduction fittings installation.

Form blocks at one end were aligned and bonded in place while the truss was still on the fixture. The form blocks in the second set were aligned and bonded after the PTS was removed from the fixture. Alignment inspections were made before and after bonding the form blocks in place.

Thirty-six axial gages for measuring cap loading characteristics were installed by Convair on the PTS, as shown in Figure 2-23. All other test instrumentation was provided by, and installed at, JSC.

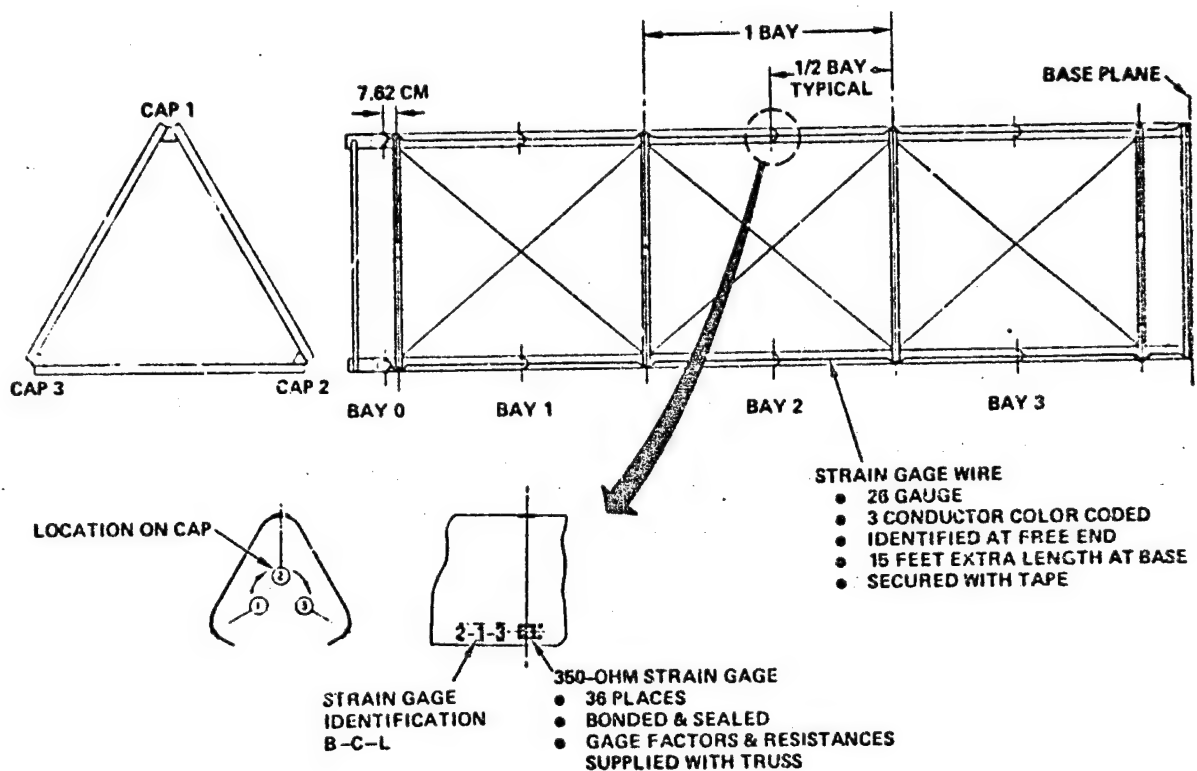


Figure 2-23. Truss strain gage installation.

2.3.3 LOCAL EFFECTS. The task flow and interrelationships for development of the local effects data are diagrammed in Figure 2-24. Local effects refers to the behavior and failure characteristics of the open section truss cap members under axial load as a column. It is known that the open sections caps are subject to local buckling, column buckling, and torsional instability when subjected to column loading. To predict local effects, analysis of local stability and column stability was performed using measured material properties. The predictions were then tested by performing short column crippling tests and long column tests. A technique for measuring local cap rotation due to the effects of torsional instability was developed and tested. The results of the column tests were to be compared with the results of the PTS compression load test to determine the end constraints or end fixity of the PTS. If the end fixity of the PTS is known, the behavior of a long truss can then be predicted.

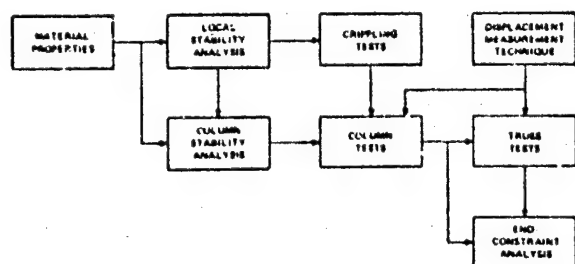


Figure 2-24. Local effects data development.

Average properties of the GR/TP material are given in Subsection 2.4.1. Since elastic flexural stiffness constants cannot be derived from the basic mechanical properties data for a single-ply woven cloth material, three flexural tests were performed on coupons in the longitudinal and transverse directions to derive the elastic constants D_{11} , D_{22} , and D_{12} . The usual test methods for determining the twisting elastic

constant D_{66} were not applicable to single-ply material. Three one-edge-free buckling tests were conducted and the value of D_{66} was computed as shown in Figure 2-25.

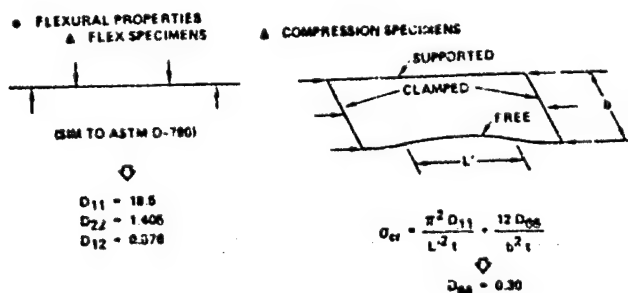


Figure 2-25. Flexural and buckling properties tests.

The structural analysis of general shells STAGS computer code was used for local stability analyses of the cap. Both bifurcation buckling and nonlinear collapse analyses were obtained using nominal thickness, 0.635 cm (0.025 in.), and the material properties. A diagram of the STAGS model is shown in Figure 2-26, including the half section used in analyses. STAGS is a finite difference code where rows and columns are defined as shown, respectively; also, coordinates and displacement components are indicated. There are four branches to the

model and 25 rows were used with a total length (L) of 63.5 cm (25 in.). The results of both the bifurcation and nonlinear collapse analyses are presented in Figure 2-27, which shows the total compression load P_c , versus the nondimensionalized end shortening, u/L . This type of plot is an expedient means of comparing analyses with test.

Two crippling tests of the cap were performed with provide the local buckling strength behavior and the crippling strength. Specimens two feet in length were used for this test and the ends were carefully potted in steel blocks to obtain uniformity of the compression load. A specimen is shown, during test, in Figure 2-28.

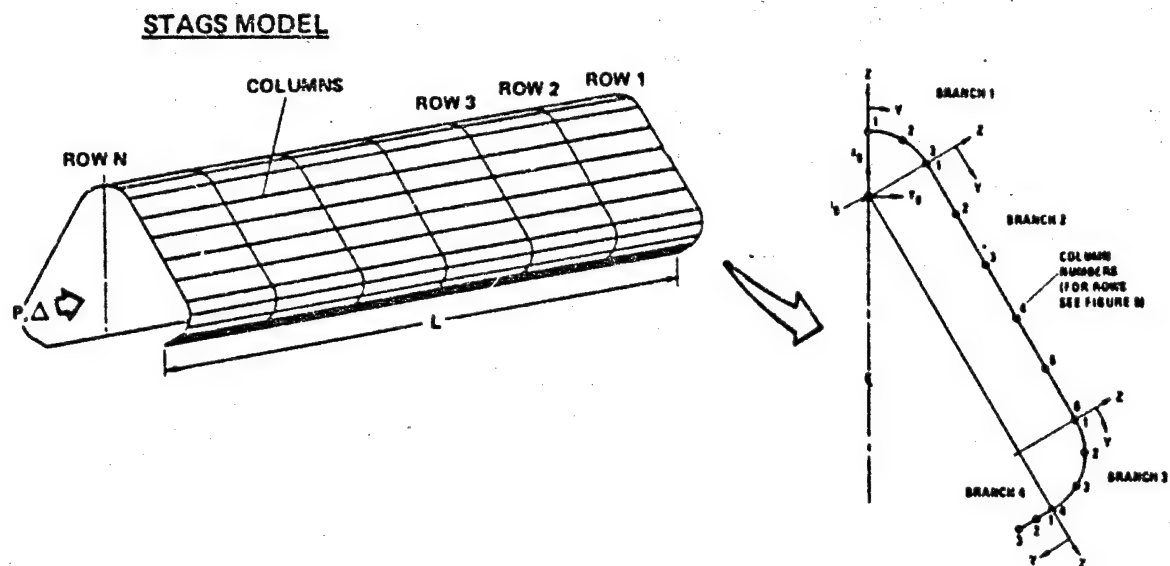


Figure 2-26. Finite-difference model for STAGS.

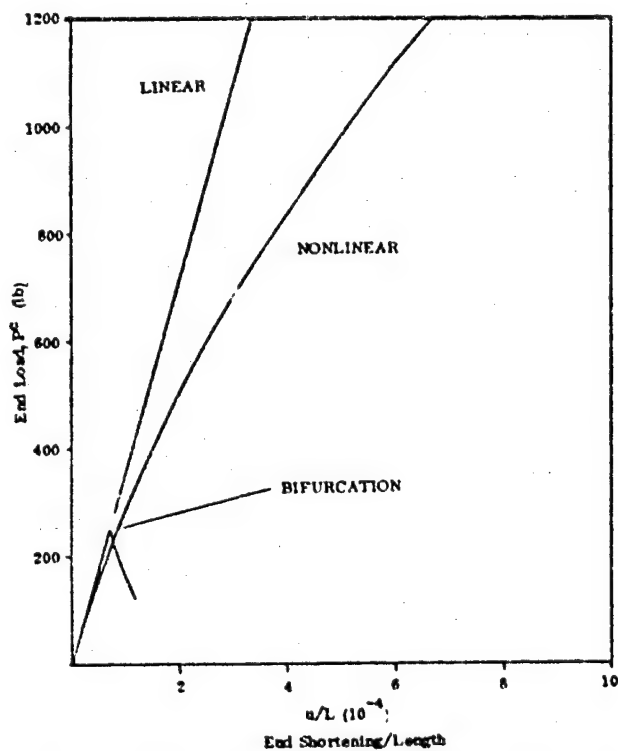


Figure 2-27. Predicted local buckling and end shortening for crippling test specimens.

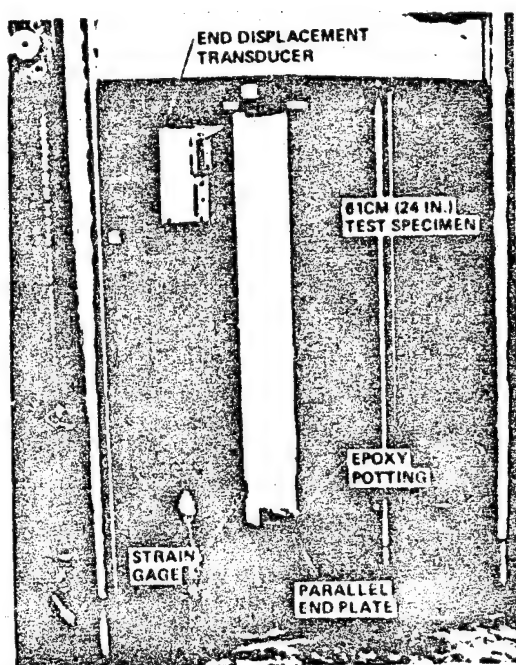


Figure 2-28. Cap column crippling test set-up.

The end-shortening plots for the two tests are presented in Figure 2-29. Both tests reached a crippling load of about 800 pounds. The bifurcation buckling loads did not compare to the STAGS analyses. The reason is that the cap varied in thickness from 0.711 - 0.940 mm (0.028 - 0.037 in.) as compared to 0.735 mm (0.025 in.) used in the analysis. This thickness variation was the result of the intermittent compaction process discussed in Subsection 2.1.1.

The calculated bifurcation buckling load may be adjusted as indicated in Figure 2-29. This resulted in good correlation between analyses and test.

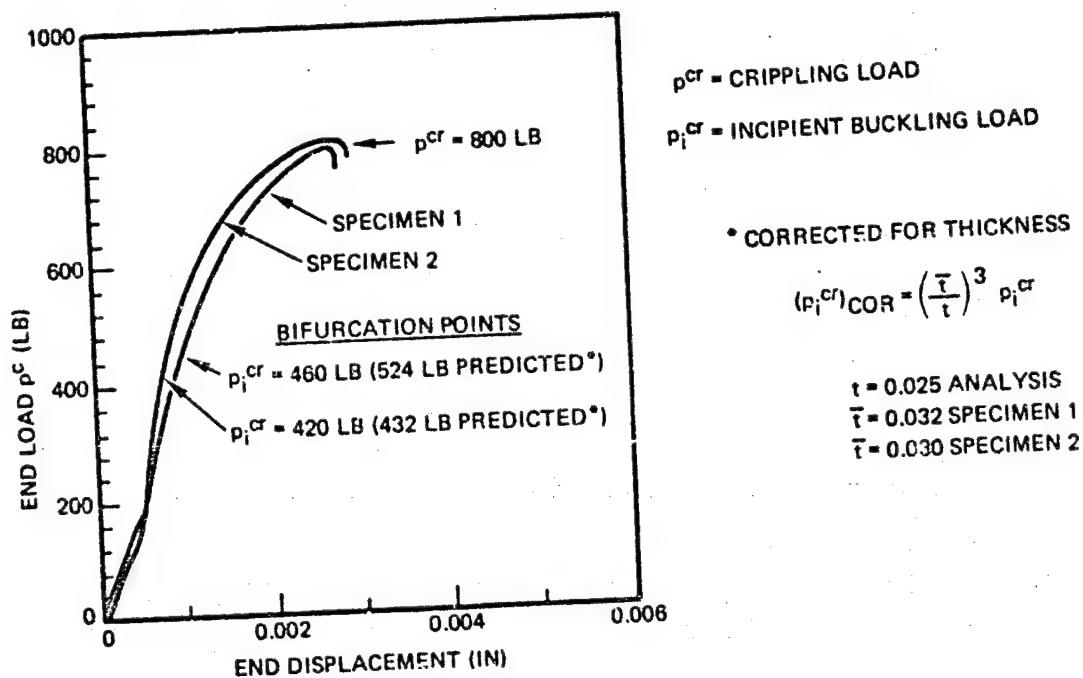


Figure 2-29. Crippling test results.

Further analysis indicates that the short column crippling strength and the long column buckling strength are virtually the same. Consequently, the critical long column load should be about 800 pounds, were it not for the effects of torsional instability. A thin-walled open section column may exhibit torsional instability when subjected to compression loading if the free length is sufficiently large. Otherwise, the member may be subject to short or long (Euler) column buckling. In some cases, the structure may be affected by the interaction of torsional and column buckling. For expediency in the stability analysis of the cap over one bay length, the effects of the crossmembers and diagonals were assumed to provide simple support at the ends and complete restraint against rotation at the ends. The STAGS computer code with the nonlinear option was chosen for this analyses. There are two options for the STAGS finite difference model.

- a. Option One is to input user-written initial imperfections that impose a maximum rotation at midspan, tapering to zero at the ends. The configuration of the imperfections is shown in Figure 2-30. Notice that these imperfections will result in torsional instability and may also impose lateral bending of the cap, which would tend to move the two free edges closer together. This analysis can be accomplished by arbitrarily assuming that the transverse flexural stiffness of the flat elements is large enough to preclude local buckling. This procedure will not affect the torsional instability analysis. In the present problem, the transverse flexural stiffness had to be eight times as large as the actual value. A half-model with 10 rows (see Figure 2-26) is sufficient for this analysis.
- b. The second option is to use the same model as described above, but accommodate local buckling of the flat sides instead of precluding it. This would require about 125 rows instead of 10 required in Option 1, so that there are a sufficient number of rows on each half-wave of the local buckling eigenvector. The local buckling model for nonlinear behavior would need an additional user-written subroutine for local imperfections to supplement the long wave imperfections discussed in Option 1.

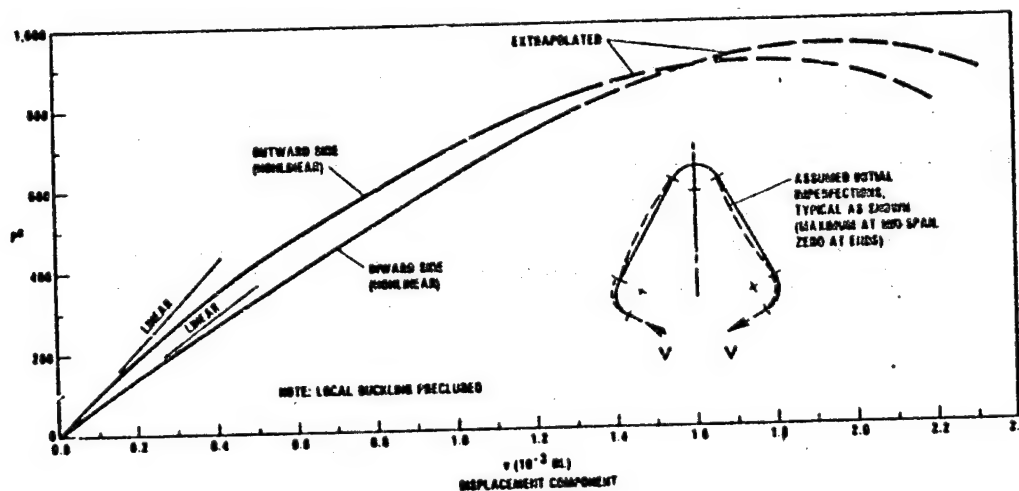


Figure 2-30. Predicted compression load versus tangential displacement of free edges due to torsional instability.

It was decided to proceed with Option 1 to minimize computer time. However, since local buckling and torsional instability were analyzed separately, interaction analysis was used to predict collapse load.

The results of the STAGS analyses for nonlinear torsional instability with flexural buckling precluded is shown in Figure 2-30. Thus, the torsional collapse load is:

$$P_T^c = 900 \text{ lb}$$

and the flexural column buckling load from the crippling tests is:

$$P_T^c = 800 \text{ lb}$$

The allowable compression collapse load, accounting for interaction effects was determined to be:

$$P_{cr}^c = 442 \text{ lb}$$

Since the initial imperfections were applied in the STAGS analyses, displacements of the free edge occurred at the outset. Accordingly, the bifurcation point for torsional instability cannot be determined from Figure 2-30. Also, a STAGS bifurcation analysis was not performed because it had been found previously to be highly unconservative, for some unknown reason.

A 244 cm cap column test specimen was potted in parallel steel end plates for the purpose of testing with a uniform comparison load. The test setup for the column test is shown in Figure 2-31.

To test for torsional instability, complete restraint to twist was provided at two locations, a distance apart equal to one bay length. These restraints were free-sliding form blocks that could be set up to allow column buckling about either principal axis. A contoured wooden stop with clearance to the outside of the cap of about 0.3 cm (0.12 in.) was provided at the center of the column for visual evidence of torsion (rotation) of the cross section and to prevent runaway torsional collapse of the specimen.

The technique used to measure cap rotation at the center is shown in Figure 2-32. A beam from a stationary 2 mW laser was reflected from a small mirror bonded to the top of the cap section. The reflected beam was projected onto a paper screen located 3.15 m (124 in.) from the mirror for test 1, and 4.27 m (168 in.) from the mirror for test 2. The laser was placed within 2.5 m (98 in.) of the mirror. Differences

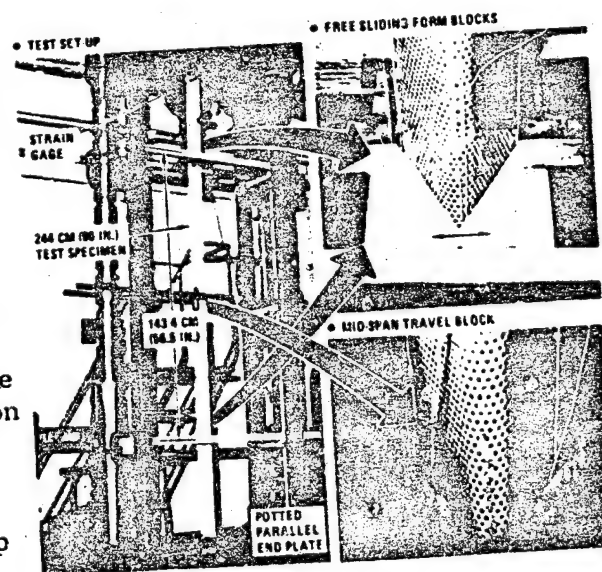
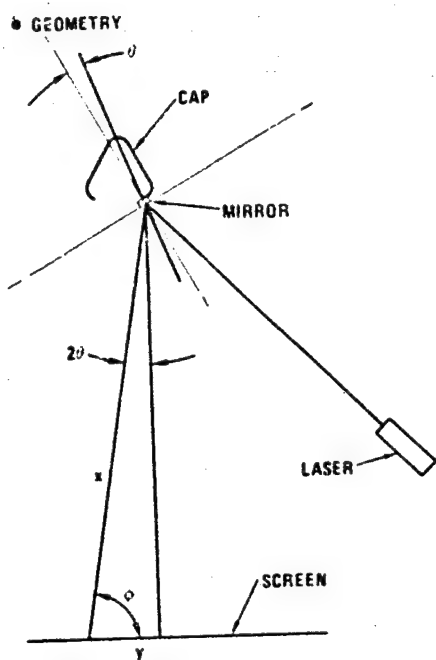


Figure 2-31. Cap column test setup.



• MIRROR ROTATION

$$\theta = \frac{1}{2} \left[\cos^{-1} \left(\frac{2x^2 - 2xy \cos \phi}{2x \sqrt{x^2 + y^2 - 2xy \cos \phi}} \right) \right]$$

Figure 2-32. Cap rotation measurement.

contacted the travel block at a load of between 375 and 400 lb. The test was terminated at this point.

in deflections of the spot on the screen were marked off as the column was loaded in 222.4 N (50 lb) increments. The apparent rotation, θ , of the cap section could then be computed.

Figures 2-33 and 2-34 show the plots of the column end displacement and apparent cap rotation versus end load for the two tests. During test 1, it became evident that the column was experiencing combined local buckling and torsional instability, due to both upward and lateral displacement of the laser beam. The beam displacements increased with each load increment. At between 400 and 450 lb, the displacement of the beam changed abruptly and the cap contacted the center travel block. The test was terminated at this point.

Test 2 was considered to be a more critical test of actual loading conditions when installed in a truss. With the cap free to flex in the weakest direction, the interaction of column buckling and torsional instability would be the most severe. During the test it was visibly observed that the cap section at mid-span was rotating and moving laterally, and the cap edges were closing together. The cap section

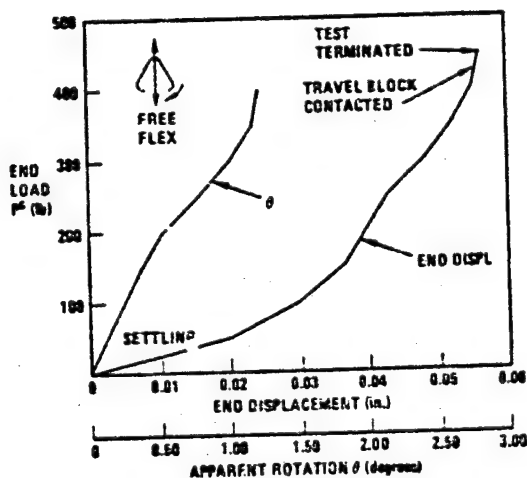


Figure 2-33. Cap column test no. 1 results.

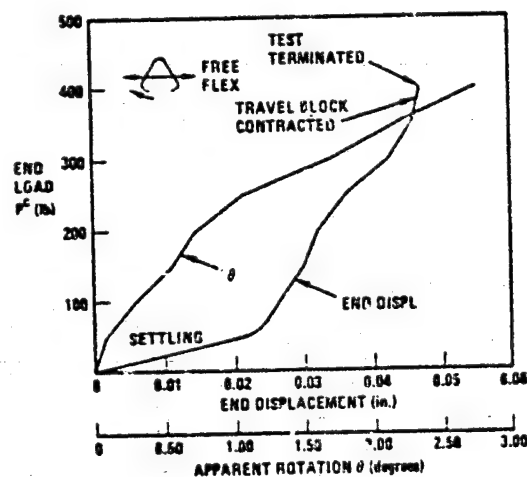


Figure 2-34. Cap column test no. 2 results.

It was not possible to show accurately what the true rotation of the cap was at mid-span. The lateral displacement had little effect on the laser beam spot displacement; however, the closing of the cap section edges could have had a significant effect on the spot displacement. It would, therefore, have been best to have placed the mirror on the apex of the cap section to preclude the effects of edge closure.

The compression collapse load is presumed to have occurred at 350 to 400 lb. Thus, there is reasonable agreement between test and theory where:

$$P_{cr}^c \text{ (experimental)} \approx 375 \text{ lb}$$

$$P_{cr}^c \text{ (theoretical)} = 442 \text{ lb}$$

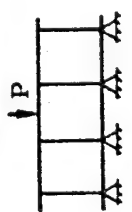


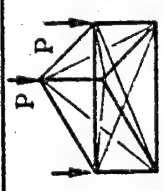
The displacement of the free edges was due to the interaction of cap rotation, local distortions, and lateral bending deflections of the cap. Insufficient nonlinear analyses were performed to obtain displacements which would correlate with the test displacements.

2.3.4 PTS TEST RESULTS. The PTS test sequences and results are summarized in Table 2-6. The PTS was subjected to four recommended tests at the JSC Structures and Mechanics Laboratory: cap transverse stiffness; torsional stiffness; torsional damping; and axial compression. Flexural stiffness and damping tests were not performed because of scheduling conflicts with Orbiter structural tests.

The fragility of the PTS was inadvertently demonstrated during test preparations when accidental contact by personnel with the truss resulted in fracture of a crossmember, two broken cords, and elongation of one cord. Repairs were performed prior to testing to replace the three damaged cords by bonding new cords to the cap members with the proper amount of tension applied. The broken crossmember was repaired by bonding a splice section of crossmember over the damaged area. These repairs were designed to restore the PTS to a level of structural performance capability needed to complete the test sequence.

The cap transverse stiffness was lower than expected, due to the contribution of the crossmembers to the total deflection. A dial indicator was installed at one crossmember station during runs 2 and 3 which showed the local deflection to be approximately 62% of the total deflection at mid-span. Cap transverse stiffness is a truss handling consideration. If used in a space construction system, the truss would be held in place and translated through retention and guide rollers at each apex. Local loading would occur through the reaction of bending moments on the truss. The deflections here should be as small as possible to ensure positive retention of the truss at all times. The test results indicate a need to increase the stiffness of the crossmembers to provide greater cap transverse stiffness.

Table 2-6. PTS Test Summary.

Test			Load Conditions							Test Results
Seq	Type	Run	Orientation	Reps	Max Value	Increment				
						Apply	Relax			
1	Cap Transverse Stiffness	1		Cap 1	2	218 N	20%	20%	Average value for 6 runs 33.5 kN/m (191.3 lb/in.) $\sigma = \pm 1.8$ kN/m (± 10.3 lb/in.)	
		Cap 2		2	218 N	20%	20%			
		Cap 3		2	218 N	20%	20%			
2	Torsional Stiffness	1		1	1	5°	20%	20%	Average value 6.7 kN-m ² (2.33×10^6 lb-in ²)	
		2		1	5°	20%	20%			
3	Torsional Damping	1		1	1	4.5°	100%	Instant	C/C _{cr} = 1.2%	
		2		1	4.5°	100%	Instant	C/C _{cr} = 3.2%		
4	Flexural Stiffness	-1	—	—	—	—	—	—	Not Run	
5	Flexural Damping	-1	—	—	—	—	—	—	Not Run	
6	Axial Compression	1		Bifurc.	1	3.34 kN	20%	—	Onset of nonlinearity occurred at 756-800N (170-180 lb) } Not Run	
		Post-Buckling		—	—	—	—			
		Ultimate		—	—	—	—			

The torsional damping test results differed, depending on the wind-up direction. The difference in damping between the clockwise run and the counterclockwise run is unexplained. Since only one run was made in each direction, it is not known if these values are repeatable. The counterclockwise test yielded more uniform data and is considered more valid than the clockwise test.

Test Sequence No. 6 of the Structural Test Plan for the PTS was conducted with the test article oriented vertically. The axial compression load was applied by a single hydraulic actuator via a ball and socket attachment to a loading plate on top of the test article. The loading plate distributed the single applied force equally to each of the three longitudinal cap members. A photograph of the test setup is shown in Figure 2-35.

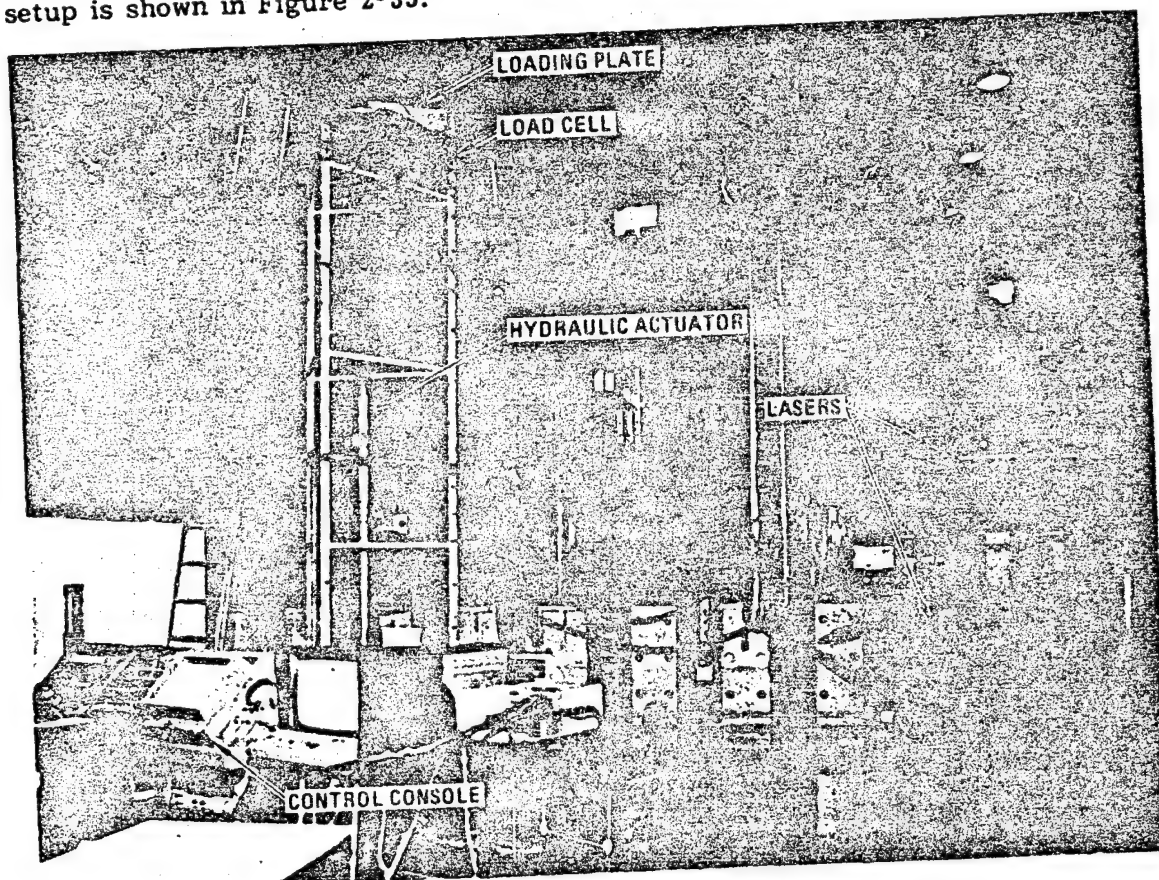


Figure 2-35. PTS axial compression test.

The test plan called for three test runs: the first of which was to determine the compressive load at which local buckling of the caps occurred; the second was to evaluate post-buckling strength; and the third run was to be a loading run to failure, to establish the ultimate compressive strength of the truss segment. The first run was successfully completed, but prior to the start of the ultimate strength run, a compressive load of unknown magnitude was suddenly and inadvertently applied by the test operator and this load resulted in failure of the caps of the test article.

There were 66 channels of instrumentation for this test, consisting of 4 load cells, 7 LVDT deflections, 52 strain gauges, and 3 acoustic emission counters, which were electronically recorded during the test. In addition to these electronically recorded measurements, three lasers were used to measure the angular rotation of the three caps.

The maximum applied compressive load for the bifurcation test run was 3.43 kN (772 lb). The load cells at the top of each cap indicated that this applied load was distributed equally to the three longitudinal caps, within about 1.5 percent. The axial deflection measurements of the caps were used during this test run to indicate the onset of initial local buckling of the caps. The axial and angular deflection versus axial load in cap no. 1 and cap no. 3 is shown in Figure 2-36. The LVDT at the top of cap no. 2 gave very erratic readings and

was discounted. From the deflection plots, it was determined that the cap load at which local buckling first appears is between 756 N and 800 N (170-180 lb). The cap strains at the maximum applied load were all relatively small (less than 500 $\mu\text{m/m}$). The magnitude of the maximum capload applied was not sufficient to produce meaningful strain gauge data.

The acoustic emissions which were monitored during the first test run showed the number of recorded emissions increased with increasing load in an orderly fashion and there was no asymptotic increase in the acoustic emission counts, which is the signal for impending failure.

Although the PTS test program was only partially completed, it yielded these important findings:

- The diagonal cord members are not easily seen when working in proximity with the truss. This makes them vulnerable to breakage. It was also found that the cords are easily broken because the cord capture weld may cause a localized weak spot right at the edge of the weld. These findings indicate the need for further improvements in the cord and weld joint design.
- The cap transverse stiffness test indicated the need to provide more stiffness at the crossmember stations to minimize the deflections of the caps at mid-bay when subjected to a local transverse load.
- The axial load test shows the truss to be structurally adequate for a SCAFE application where maximum predicted loads on the cap members

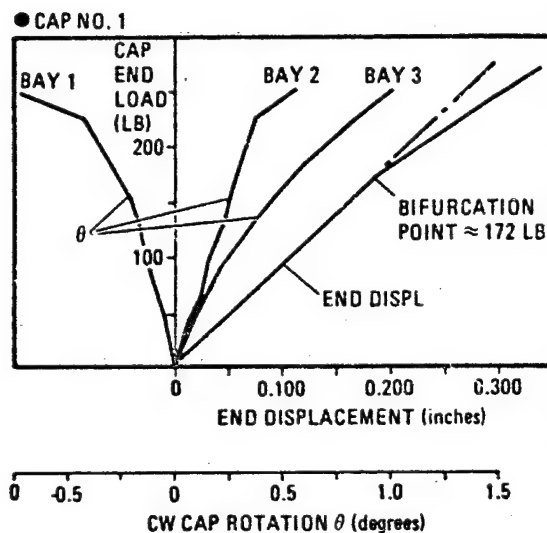


Figure 2-36. Axial load versus cap displacement and rotation.

are less than 445 N (100 lb). Further testing would reveal to what extent the truss could operate in the post-buckling load range without damage or deterioration. Also, more testing and analysis of material characteristics and open section cap members would lead to much more precise methods of predicting the structural performance of the truss.

2.4 GRAPHITE COMPOSITE MATERIAL

In addition to the forming, welding, truss manufacture, and local effects tasks, Convair provided samples of graphite/thermoplastic (GR/TP) consolidated strip material for testing in a NASA/LaRC material space environmental test program. The material used in this program, the material provided to LaRC, and the nature of the environmental tests which were performed by LaRC are described below.

2.4.1 FORMING, WELDING, & TRUSS MATERIAL. The GR/TP composite material used in each of the program tasks reported in the preceding sections is a hybrid, single-ply woven graphite and glass cloth impregnated with Union Carbide's P-1700 polysulfone resin and coated with TiO₂ pigmented P-1700 resin. The material characteristics are as shown in Figure 2-37. The extensional properties were measured at room temperature after consolidation.

All forming, welding, and truss fabrication was performed with strip material from the same batch. This material was procured from Fiberite Corp., and delivered to Convair in March 1979. It was the fourth in a series of material designs developed and tested by Convair in conjunction with automated in-space fabrication technology IRAD.

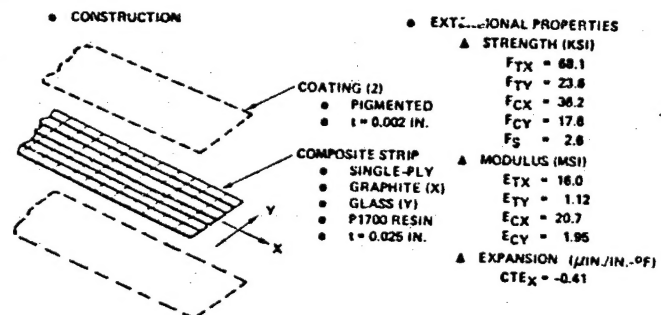


Figure 2-37. Material characteristics.

2.4.2 SPACE ENVIRONMENTAL TEST MATERIAL.

The GR/TP composite material supplied to NASA/LaRC for their space environmental test program was similar to the material used in the forming, welding, and truss fabrication tasks. The 968 cm² (150 in.²) of consolidated strip material delivered to NASA/LaRC on 7 November 1979 was taken from the previous batch of hybrid/graphite/glass polysulfone composite material tested by Convair which was of a different weave and fiber content than the material used for other program tasks. NASA/LaRC planned to perform flexure tests on miniature material coupons to determine mechanical properties before and after exposure to the following radiation levels:

- 1 MeV electrons
- 1×10^{10} rads (≈ 30 years at GEO)
- 20°C and 120°C each exposure

The results of this testing are to be published by LaRC.

3

CONCLUSIONS AND RECOMMENDATIONS

3.1 CONCLUSIONS

Table 3-1 presents conclusions in the subject sequence of the preceding text.

Table 3-1. Program conclusions.

● CONCLUSIONS
<ul style="list-style-type: none">▲ The Rolltrusion process represents a viable and efficient solution to the problem of roll forming graphite composite material for in-space fabrication of large space structures.▲ Minor irregularities observed in cap sections can be corrected by simple changes to the heater reflectors.▲ Curvature of cap members can be resolved by using strip material of uniform thickness.▲ The lack of capability to produce high quality preprocessed GR/TP strip material will impede progress in beam builder and large space structures technology in two ways:<ul style="list-style-type: none">(1) Small batch production will become prohibitively expensive as greater quantities are required to support development.(2) Improper pre-processing techniques will preclude accurate determination of material structural and long-term operating behavior.▲ The baseline SCAFEDS beam builder drive speed produced no speed-related defects in roll formed caps.▲ The Rolltrusion process can be adapted to higher drive speeds.
● ULTRASONIC WELDING TECHNOLOGY
<ul style="list-style-type: none">▲ Ultrasonic welding in vacuum produced no identifiable effect on weld strength or resin flow characteristics.▲ Welding GR/TP material which has been properly conditioned to remove moisture and volatiles produces no outgassing in vacuum.▲ Vacuum-compatible ultrasonic welder electronic amplifiers and controllers must be developed for the beam builder.▲ Piezoelectric ultrasonic transducers operate in vacuum when properly evacuated.▲ Ultrasonic welding in vacuum produced no change in the efficiency of the welder and no significant heating effects on the weld horn or transducer.▲ Heat is conducted away from the weld primarily in the direction of the graphite fibers, and the rate of cooling is not significantly different between welds produced in air and in vacuum.▲ Welder performance is affected by gravity but would not be affected by zero-gravity.▲ Gravity effects on the welder performance can be compensated for by adjusting weld pressure and weld time and the stiffness of the weld horn can be changed to preclude gravity effects.▲ The weld power characteristic during weld is sensitive to material thickness and surface conditions, and the amount of weld energy applied correlates well with weld strength. Weld energy and weld power profile monitoring should be considered as in-process quality control parameters for the beam builder system.▲ A beam builder ultrasonic welder will require automatic frequency compensation for weld horn temperature changes.
● PROTOTYPE TEST TRUSS
<ul style="list-style-type: none">▲ Minor modification of the truss welding horn is required to allow the cord to be maintained in full tension during welding without breaking.▲ Fabrication and assembly of the PTS proved that the SCAFEDS beam builder concept is sound and no major technical problems exist that preclude its development.▲ The incipient buckling loads measured for the crippling test specimens showed good correlation with the predicted load, corrected for thickness.▲ The critical column buckling load for cap members would be nearly the same as the short column crippling strength in the absence of torsional instability.▲ Interaction analysis of the combined effects of column buckling and torsional instability for the open section cap member when compared with the column test results, showed only fair correlation. A more perfect test specimen and a STAGS analysis which accommodates both torsional instability and local buckling is required to demonstrate that the load effects analysis is producing reasonable results.

3.2 RECOMMENDATIONS

The work completed on the Graphite Composite Truss Welding and Cap Section Forming Subsystems program indicates the need for continued key technology and hardware development as recommended in Table 3-2, if a truly useable beam builder and large space structures construction system is to become a reality.

Table 3-2. Recommendations.

● BEAM BUILDER TECHNOLOGY

- ▲ Design, develop, manufacture, and test a flight qualifiable cap forming module as defined in JSC specifications BB-SS-100 and BB-CFS-101, to accomplish the following:
 - (1) Conduct ground test and evaluation of vacuum and gravity effects.
 - (2) Develop a precision cap drive and control technique.
 - (3) Optimize heaters, temperature sensor, and temperature controls for an operational space system.
 - (4) Conduct in-space cap forming experiments to ensure flight and in-space operational compatibility.
- ▲ Design, develop, manufacture, and test a flight qualifiable ultrasonic welder for the beam builder per the requirements of JSC specification BB-BJS-101, to accomplish the following:
 - (1) Optimize weld head size, weight, and efficiency.
 - (2) Provide a space-compatible weld power and control module.
 - (3) Incorporate automatic in-process quality assurance functions and assess reliability of welds.
 - (4) Conduct ground test and evaluation of the effects of long-term operation of the welder in vacuum.
 - (5) Conduct in-space ultrasonic welding experiments to ensure flight and in-space operational compatibility.

● GRAPHITE/THERMOPLASTIC MATERIALS TECHNOLOGY

- ▲ Continue the analysis and test of single-ply woven fabric material as follows:
 - (1) Determine the effects of manufacturing techniques on material properties.
 - (2) Conduct experiments to assess how closely the coefficient of thermal expansion of the material can be controlled and how stable it remains with time, temperature, and load.
 - (3) Determine the fatigue of repeated loading and thermal cycling.
 - (4) Establish the behavioral characteristics of single-ply versus laminated GR/TP materials.
- ▲ Establish manufacturing requirements for GR/TP strip material which will define the techniques required for continuous compaction, coating, conditioning, and quality assurance.

● LARGE SPACE STRUCTURES TECHNOLOGY

- ▲ Continue to analyze, fabrication, and test prototype structure and structural elements.
 - (1) Test cap members for post-buckling fatigue life.
 - (2) Perform a STAGS analysis of the combined effects of local buckling, column buckling, and torsional instability on cap load carrying capability.
- ▲ Conduct tests to determine the endurance of truss weld joints under cyclic loading and long-term static loading.

**END
DATE
FILMED**

MAY 27 1981